

Coherent Matter Wave Transport in Speckle Potentials

R C Kuhn^{1,2}, O Sigwarth¹, C Miniatura^{2,3}, D Delande⁴ and C A Müller¹

¹ Physikalisches Institut, Universität Bayreuth, D-95440 Bayreuth

² Institut Non Linéaire de Nice, UNSA, CNRS, 1361 route des Lucioles, F-06560 Valbonne

³ Department of Physics, Faculty of Science, National University of Singapore, Singapore 117542

⁴ Laboratoire Kastler Brossel, Université Pierre et Marie Curie-Paris 6, 4 Place Jussieu, F-75005 Paris

E-mail: cord.mueller@uni-bayreuth.de

PACS numbers: 03.75.Kk, 42.25.Dd, 73.20.Fz

Abstract. This article studies multiple scattering of matter waves by a disordered optical potential in two and in three dimensions. We calculate fundamental transport quantities such as the scattering mean free path ℓ_s , the Boltzmann transport mean free path ℓ_B , and the Boltzmann diffusion constant D_B , using a diagrammatic Green functions approach in the weak scattering regime. Coherent multiple scattering induces interference corrections known as weak localization which entail a reduced diffusion constant. We derive the corresponding expressions for matter wave transport in an correlated speckle potential and provide the relevant parameter values for a possible experimental study of this coherent transport regime, including the critical crossover to the regime of strong or Anderson localization.

1. Introduction

The observation of the first gaseous Bose-Einstein condensates in 1995 and, a few years later, of the first gaseous ultra-cold fermion gases constitutes a major achievement in the field of atomic physics. Loading ultra-cold degenerate gases, be it fermions, bosons, or fermion-boson mixtures into optical lattices has opened fascinating new perspectives for the study of condensed-matter quantum physics [1–4]. A particularly promising line of research is the experimental and theoretical study of quantum phase transitions [5]. Indeed, the high degree of control and precision achieved in these experiments has allowed systematic studies of physical phenomena that are observed until now mostly in solid-state systems.

A natural evolution in this domain is the investigation of the influence of *disorder* [6] which can induce a Bose-glass phase for strongly interacting bosons [7], and a Lifshitz glass [8] or an Anderson glass [9] for weaker interaction. Experimentally, a major milestone has been reached with the realization of quasi-1D condensates evolving in a speckle light field [10–14]. Such disordered optical potentials can be easily generated and their statistical properties are well known [15]. In two dimensions, atomic diffusion has been studied in optical quasi-crystals with five-fold symmetry for atomic clouds in the dissipative regime [17] and Bose-Einstein condensates [18] covering the intermediate regime between ordered and completely disordered systems. Most recently the experimental observation of the onset of the Bose glass phase for ultra-cold atoms in a bichromatic optical lattice has been reported [16].

Disorder has long proven to be a crucial ingredient to understand coherent transport properties. The most prominent example is the *weak localization* phenomenon in mesoscopic physics [19–21], which has been studied extensively for electrons [22, 23] and for classical waves [24, 25]. Weak localization arises from interference between multiply scattered waves in a random medium. This interference survives the configuration average over many realizations of disorder and reduces the conductivity that enters the Drude model for electron transport [26] and the diffusion constant of classical radiative transport theory [27, 28]. Disorder can even induce a metal-insulator transition, known as the strong (or Anderson) localization transition [29–33], that has been studied extensively in the framework of the tight binding model [34, 35]. In the localized regime the quantum states cease to extend over the whole system and become spatially localized with the consequence that quantum transport through the system is exponentially suppressed.

From a theoretical point of view, atom transport shares many similarities with the radiative transfer theory [36] and even more with electron transport theory [20, 21]. Unfortunately, the unambiguous observation of wave localization phenomena for matter waves is difficult if the quantum evolution is interaction-dominated. But there are several ways to achieve the interaction-free regime: for example, one can let the ultra-cold gas first expand, so as to decrease its spatial density, before switching on the speckle potential. A more elaborate way would be to tune the two-body interactions by using a Feshbach resonance [4, 37]. In this case, by scanning a magnetic field, one can continuously go from the independent-particle regime to the strongly interacting regime. This offers the possibility to study in a controlled way how localization is affected by interactions.

In this paper we focus on the impact of disorder in the independent-particle regime and discard both atom-atom interactions and quantum statistical effects. Such a situation can be reached with ultra-cold atoms produced from a Bose-Einstein condensate or a Fermi degenerate gas by opening the trap and decreasing the atomic density far below the quantum degenerate regime. Our results therefore apply to non-interacting ultra-cold gases at low densities. Our paper is inspired by Vollhardt and Wölfle’s seminal work on electron transport theory [38] and is an extension of our previously published results on localization of matter waves in two-dimensional speckle potentials [39]. We calculate experimentally relevant transport quantities, such as the scattering mean free path, the transport mean free path, the diffusion constant and the weak localization corrections, treating the two- and three-dimensional cases in parallel. Contrary to the case of 1D transport studied recently by Sanchez-Palencia et al. [40] to which this theory can also be applied, the 2D and 3D cases are of special interest because 3D allows for the Anderson localization transition at a finite disorder strength, whereas 2D is the marginal case (the lower critical dimension) where analytical results are particularly important. We show that it should be possible, with the current experimental state of the art, to observe weak and strong localization effects provided that phase-breaking mechanisms are under control.

The paper is organized as follows: in section 2 we discuss the optical potential and its statistical properties and we derive the dimensionless Schrödinger equation which governs the atomic motion in the speckle potential. Sections 3 and 4 (and corresponding appendices containing the technical details) are intended to give an introduction to the diagrammatic perturbation theory. We obtain analytic expressions for the configuration-averaged propagator and the scattering mean free path as well as for the intensity relaxation kernel and the transport mean free path. Section 5 (and corresponding appendices) are devoted to the calculation of quantum corrections to classical transport. We derive the reduced diffusion constant in 2 and 3D, and study the strong localization onset.

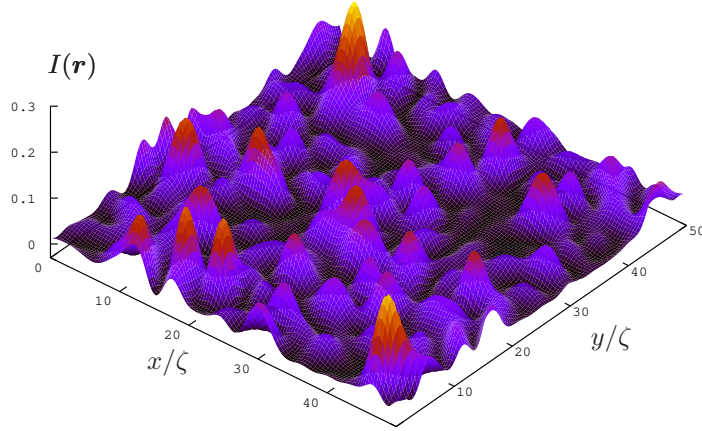


Figure 1. Intensity plot of a 2D speckle pattern, numerically generated as described by Horak et al. [41]. The positions x and y are given in units of the speckle correlation length ζ .

2. Atomic Hamiltonian Dynamics

In the present section, we formulate the general description of the single-particle dynamics for noninteracting cold atoms in disordered speckle potentials.

2.1. Light shifts

When an atom is exposed to electromagnetic radiation, it is polarized, and its energy levels are shifted. In the case of interaction with a laser light field, these energy shifts are called light shifts [42]. In the dipolar approximation, the light shifts are proportional to the field intensity evaluated at the center-of-mass of the atom. If the field intensity is space dependent, so are the light shifts, and a moving atom experiences dipolar forces altering its trajectory. By conveniently tailoring the space and time dependence of the light field, one can produce a great variety of potentials for guiding the atomic motion.

In the present paper, we consider the interaction of a two-level atom (mass m , internal electronic ground state $|g\rangle$, energy separation $\hbar\omega_A$ to the excited state $|e\rangle$ with natural energy linewidth $\hbar\Gamma$, electric dipole moment d_e) with a monochromatic electromagnetic laser field $\mathcal{E}(\mathbf{r})$ (wave number k_L , wavelength $\lambda_L = 2\pi/k_L$, angular frequency $\omega_L = ck_L$). The two-level description is appropriate for atoms like strontium [43] with a nondegenerate electronic ground state or atoms like rubidium whose ground-state degeneracy is lifted by a strong magnetic field [44].

The coupling strength between the atom and the electromagnetic laser field is described by the angular Rabi frequency $\hbar\Omega(\mathbf{r}) = -d_e\mathcal{E}(\mathbf{r})$. The detuning $\delta_L = \omega_L - \omega_A$ from an optical resonance is generally small compared to the transition frequency, $\delta_L \ll \omega_L$. In this case, anti-resonant interaction terms can be ignored (rotating-wave approximation) [45]. Hereafter, we assume that the atom is initially prepared in its internal ground state, and that the laser detuning satisfies $\delta_L \gg \Gamma, \Omega_L$, where Ω_L is the mean value of the Rabi frequency. The transition amplitude to the excited state is then small, and the ground-state light shift at position \mathbf{r} caused by the laser intensity $I(\mathbf{r}) = (\frac{1}{2}\epsilon_0 c)|\mathcal{E}(\mathbf{r})|^2$ is

$$V(\mathbf{r}) \approx \frac{\hbar|\Omega(\mathbf{r})|^2}{4\delta} = \frac{\hbar\Gamma}{8} \frac{\Gamma}{\delta_L} \frac{I(\mathbf{r})}{I_s}. \quad (1)$$

The saturation intensity I_s is a characteristic of the atom under consideration. The atomic motion is then governed by the effective Hamiltonian $H = \mathbf{p}^2/2m + V(\mathbf{r})$.

The atomic evolution is purely Hamiltonian only up to some time τ_i : because of the coupling to the photon vacuum fluctuations, the light-atom interaction also contains a dissipative term which limits the temporal coherence of the atomic wave function. The average inelastic scattering rate or inverse inelastic time can be calculated using the optical Bloch equations [42] and reads

$$\gamma_i = \frac{1}{\tau_i} \approx \frac{\Gamma}{\delta_L} \frac{V_L}{\hbar}. \quad (2)$$

Here $V_L = \overline{V(\mathbf{r})}$ is the average light shift, given in terms of the average intensity $I_L = \overline{I(\mathbf{r})}$:

$$V_L = \frac{\hbar\Gamma}{8} \frac{\Gamma}{\delta_L} \frac{I_L}{I_s}. \quad (3)$$

Coherent interference of multiple scattering amplitudes can affect the atomic dynamics if this dissipation is controlled at an arbitrarily low rate by using a sufficiently far-detuned speckle field $\delta_L \gg \Gamma$ at constant average potential height V_L .

2.2. Speckle potential

A monochromatic speckle pattern with random intensity and phase variations defines a disordered potential $V(\mathbf{r})$ as displayed in figure 1. The corresponding electric field $\mathcal{E}(\mathbf{r})$ is a superposition of many complex field amplitudes with zero mean. Then, as stated by the central limit theorem, the real and imaginary parts of the field amplitude are uncorrelated Gaussian random variables [15]. Thanks to the Gaussian moment theorem [46], all correlation functions of the electric field can be expressed in terms of the pair correlation function $\mathcal{P}_{\mathcal{E}}(\mathbf{r}, \mathbf{r}') = \overline{\mathcal{E}^*(\mathbf{r})\mathcal{E}(\mathbf{r}')}$. The ensemble average typically restores translational invariance, $\mathcal{P}_{\mathcal{E}}(\mathbf{r}, \mathbf{r}') = \mathcal{P}_{\mathcal{E}}(\mathbf{r} - \mathbf{r}')$, and one defines the dimensionless field correlation function or so-called complex degree of coherence [47]:

$$\gamma_d(\mathbf{r}) = \frac{\overline{\mathcal{E}^*(\mathbf{r} + \mathbf{r}')\mathcal{E}(\mathbf{r}')}}{|\overline{\mathcal{E}(\mathbf{r})}|^2}. \quad (4)$$

The index $d = 2, 3$ indicates that the correlation function depends on the choice of a two- or three-dimensional geometry as discussed below. Since the light-shift potential (1) is proportional to the *square* of the field, the speckle potential itself does *not* have a Gaussian distribution. Nevertheless, because of the Gaussian character of the underlying field, all potential correlation functions can be split down to sums of products of the field correlation function (4). The potential pair correlation function $\overline{V(\mathbf{r}')V(\mathbf{r}' + \mathbf{r})}$ is proportional to the fourth-order field correlation $\overline{\mathcal{E}^*(\mathbf{r}')\mathcal{E}(\mathbf{r}')\mathcal{E}^*(\mathbf{r}' + \mathbf{r})\mathcal{E}(\mathbf{r}' + \mathbf{r})}$. It is given by

$$\overline{V(\mathbf{r}')V(\mathbf{r}' + \mathbf{r})} = V_L^2 [1 + |\gamma_d(\mathbf{r})|^2]. \quad (5)$$

Obviously, the potential dispersion is proportional to the average potential value V_L itself. We rewrite the light-shift potential as $V(\mathbf{r}) = V_L [1 + \delta V(\mathbf{r})]$ such that the dimensionless fluctuations $\delta V(\mathbf{r})$ have the reduced two-point correlation function

$$\mathcal{P}_d(\mathbf{r}) = \overline{\delta V(\mathbf{r}')\delta V(\mathbf{r}' + \mathbf{r})} = |\gamma_d(\mathbf{r})|^2. \quad (6)$$

$\mathcal{P}_d(\mathbf{r})$ is normalized such that $\mathcal{P}_d(0) = 1$ and decays to zero over a characteristic spatial scale ζ known as the correlation length of the speckle potential. As shown below, ζ is a crucial parameter for the dynamics of the cold atoms in the speckle potential.

A two-dimensional ($d = 2$) speckle as displayed in figure 1 can be produced by reflection of a laser from a rough surface or by transmission through a phase mask [48]. In the far-field $z \gg R$ from the phase mask, where z denotes the distance from the phase mask to the observation plane and R denotes the radius of the phase mask, the speckle interference pattern can be regarded as quasi two-dimensional since the speckle grains are very elongated in the z -direction, orthogonal to the illuminated surface. Confining atoms in the plane transverse to z in the far-field thus realizes a 2D situation. A uniformly illuminated circular phase mask with radius R yields a complex degree of coherence that takes the following form for small relative distances $r \ll z$ [15]

$$\gamma_2(\mathbf{r}) = 2 \frac{J_1(\alpha k_L r)}{\alpha k_L r}. \quad (7)$$

$J_1(x)$ denotes the first-order Bessel function. The geometrical factor $\alpha \approx R/z \ll 1$ is the numerical aperture of the imaging device; a typical order of magnitude in recent experiments is $\alpha \approx 0.1$ [10] or better, $\alpha \approx 0.45$ [49]. The speckle fluctuations originate from the coherent superposition of purely monochromatic wave vectors. This implies a diffraction limit: two points in the speckle field are correlated if sufficiently close to each other, $\lim_{r \rightarrow 0} \gamma_2(\mathbf{r}) = 1$. In the 2D case, the correlation function $\gamma_2(\mathbf{r})$ decreases to zero over a characteristic length scale $\zeta = 1/\alpha k_L = \lambda_L/2\pi\alpha$ such that the potential fluctuations are uncorrelated only for distances larger than ζ .

To produce a three-dimensional ($d = 3$) disordered configuration, the speckle grains should be obtained as the interference pattern of many wave vectors spanning the largest possible angular aperture. Ideally, this situation corresponds to the interference pattern obtained inside a closed optical cavity, e.g., an integrating sphere. The complex degree of coherence is then given by [50]

$$\gamma_3(\mathbf{r}) = \frac{\sin(k_L r)}{k_L r}, \quad (8)$$

where the correlation length is now $\zeta = 1/k_L$, corresponding to a numerical aperture $\alpha \rightarrow 1$.

Another possibly interesting configuration is provided by the speckle field at the proximity of a rough interface illuminated by monochromatic coherent light [51]. Due to the contributions of *evanescent* components, the average intensity then decreases exponentially with the distance z to the surface. If the surface is rough on short scales, the near-field speckle correlation length ζ is smaller than λ_L , which is impossible for far-field speckle patterns. Experimentally, one would have to bring the atoms sufficiently close to the surface in a controllable way and restrict the dynamics to a plane parallel to the surface [52]. This situation deserves a special study and will not be considered in the following.

A popular model for disordered potentials in the quantum transport literature is a spatially δ -correlated potential with a Gaussian distribution of potential strength. The previous considerations show that a monochromatic speckle potential is neither δ -correlated nor Gaussian. However, only the potential fluctuations as seen by the moving atoms are relevant for the atomic dynamics. We will see in the following that speckle fluctuations appear effectively δ -correlated only when the atomic de Broglie wavelength is much larger than the correlation length ζ . Attaining this quantum regime requires sub-recoil cooling techniques.

2.3. Dimensionless Schrödinger Equation

The correlation length ζ of the speckle fluctuations defines a natural physical length scale. In turn, it also defines natural scales for momentum, wave number, velocity, energy, angular

frequency, and time:

$$p_\zeta = \hbar k_\zeta = mv_\zeta = \frac{\hbar}{\zeta}, \quad E_\zeta = \hbar\omega_\zeta = \frac{\hbar}{\tau_\zeta} = \frac{\hbar^2}{m\zeta^2}. \quad (9)$$

In the 3D-speckle case (8), one has $\zeta = k_L^{-1}$ such that $v_\zeta = \hbar k_L/m = v_R$ is the familiar atomic recoil velocity, whereas $E_\zeta = 2E_R$ is twice the atomic recoil energy $E_R = \frac{1}{2}mv_R^2$. In the 2D-speckle case (7), $\zeta = (\alpha k_L)^{-1}$ and $v_\zeta = \alpha v_R \ll v_R$, whereas $E_\zeta = 2\alpha^2 E_R \ll E_R$. Scaling all dynamical variables with these units ($\mathbf{k} = \mathbf{p}/\hbar$ is the wave vector of the atom),

$$\boldsymbol{\rho} = \mathbf{r}/\zeta, \quad \tau = t/\tau_\zeta, \quad \boldsymbol{\kappa} = \mathbf{k}/k_\zeta, \quad \varepsilon = E/E_\zeta, \quad (10)$$

the Schrödinger equation reappears in the dimensionless form $i\partial_\tau|\psi\rangle = H|\psi\rangle$ with the Hamiltonian

$$H = \frac{\boldsymbol{\kappa}^2}{2} + \eta + \eta\delta V(\boldsymbol{\rho}). \quad (11)$$

In the rescaled units, the canonical commutator reads $[\boldsymbol{\rho}, \boldsymbol{\kappa}] = i$. The parameter η is the strength of the potential fluctuations in units of the correlation energy,

$$\eta = \frac{V_L}{E_\zeta} = \frac{\hbar\Gamma}{8E_\zeta} \frac{\Gamma}{\delta_L} \frac{I_L}{I_s}. \quad (12)$$

The constant term η in the Hamiltonian (11) can be reabsorbed by fixing the origin of energies at V_L . In spatial representation and rescaled units, the stationary Schrödinger equation at energy ε is now:

$$\left[\frac{1}{2} \nabla_{\boldsymbol{\rho}}^2 + \varepsilon - \eta\delta V(\boldsymbol{\rho}) \right] \psi(\boldsymbol{\rho}) = 0. \quad (13)$$

The 2-point correlation functions of the potential fluctuations in our rescaled units are

$$\mathcal{P}_2(\boldsymbol{\rho}) = \left[2 \frac{J_1(\rho)}{\rho} \right]^2, \quad (14a)$$

$$\mathcal{P}_3(\boldsymbol{\rho}) = \left[\frac{\sin(\rho)}{\rho} \right]^2. \quad (14b)$$

The equation (13) differs from the Helmholtz equation obtained for classical electromagnetic waves propagating in random dielectric media. In our case the potential fluctuations do not depend on energy. Hence the treatment for matter waves (be it atoms or electrons) is much simpler than for classical waves, where this energy dependence implies significant corrections to dynamical quantities such as the transport speed of light [25].

3. Effective Medium

The states of a wave scattered by a disordered potential are different from one realization of disorder to another. As a consequence, only expectation values obtained by averaging over many such realizations provide a useful characterization of the transport processes at work. In the language of standard quantum transport, tracing out the speckle impurities leads to a dispersion relation with finite spectral width γ_κ for the plane-wave states $|\boldsymbol{\kappa}\rangle$. Equivalently, but put into the language of atom optics, averaging over speckle realizations introduces an effective medium that is characterized by a complex wave vector $\boldsymbol{\kappa}(\varepsilon)$ for the propagating matter wave at energy ε . In this section, we calculate the dispersion relation in the weakly disordered regime where diagrammatic perturbation theory [20, 21, 53] proves particularly powerful. This theory is well known for the description of classical waves in a medium with a fluctuating index of refraction or the transport of electrons in a disordered metal. However, in

contrast to point-like impurities encountered for the scattering of electrons, the fluctuations of the optical potential exhibit spatial correlations leading to anisotropic scattering. In this sense the scattering of atomic matter waves in a speckle potential shares many similarities with the scattering of light in nematic liquid crystals where correlations between thermal fluctuations of the nematic director play an important role [54].

3.1. Retarded Green operator

The retarded Green operator or resolvent $G(\varepsilon)$ for the stationary Schrödinger equation (13) at reduced energy ε is the Fourier transform of the forward time evolution operator $\Theta(\tau)U(\tau) = \frac{i}{2\pi} \int d\varepsilon G(\varepsilon) e^{-i\varepsilon\tau}$, with the Heaviside function $\Theta(\tau)$. The Green operator satisfies the equation

$$G(\varepsilon) = G_0(\varepsilon) + G_0(\varepsilon) \eta \delta V G(\varepsilon). \quad (15)$$

The free retarded Green operator $G_0(\varepsilon) = [\varepsilon - H_0 + i0^+]^{-1}$ is diagonal in momentum space with propagator matrix elements $\langle \kappa' | G_0(\varepsilon) | \kappa \rangle = (2\pi)^d \delta(\kappa - \kappa') G_0(\kappa, \varepsilon)$, where $\delta(\kappa) = \delta(\kappa_1) \cdots \delta(\kappa_d)$, and

$$G_0(\kappa, \varepsilon) = [\varepsilon - \kappa^2/2 + i0^+]^{-1}. \quad (16)$$

Iteration of (15) yields the usual Born series (suppressing energy arguments for brevity)

$$G = G_0 + \eta G_0 \delta V G_0 + \eta^2 G_0 \delta V G_0 \delta V G_0 + \dots \quad (17)$$

Taking the configuration average of the series, one obtains

$$\overline{G} = G_0 + \eta^2 G_0 \overline{\delta V G_0 \delta V} G_0 + \eta^3 G_0 \overline{\delta V G_0 \delta V G_0 \delta V} G_0 + \dots, \quad (18)$$

where the linear term in η vanishes because $\overline{\delta V} = 0$. It appears that knowing the average resolvent requires to calculate all higher-order correlation functions of the potential fluctuations δV . However, one is interested in determining the effect of the disorder on the energy levels $\varepsilon(\kappa)$. To this end, the Born series is recast into the following form, known as the Dyson equation:

$$\overline{G} = G_0 + G_0 \Sigma G_0 + G_0 \Sigma G_0 \Sigma G_0 + \dots = G_0 + G_0 \Sigma \overline{G}. \quad (19)$$

The retarded self-energy operator $\Sigma(\varepsilon)$ contains all irreducible correlation functions, i. e. correlations that cannot be split into products of independent factors by suppressing a single propagator G_0 [55]. Recognizing a geometric series, one can formally solve the Dyson equation as $\overline{G}(\varepsilon) = [G_0(\varepsilon)^{-1} - \Sigma(\varepsilon)]^{-1}$.

The average over many realizations of disorder restores translational invariance. Consequently, $\overline{G}(\varepsilon)$ is diagonal in momentum space just like the free-space propagator $G_0(\varepsilon)$. Since the disordered potential also preserves space isotropy on average, as exemplified by the scalar correlation functions (7) and (8), the propagator matrix elements $\overline{G}(\kappa, \varepsilon)$ in momentum space can only depend on the momentum modulus $\kappa = |\kappa|$. The same conclusion holds for the self-energy $\Sigma(\kappa, \varepsilon)$ such that

$$\overline{G}(\kappa, \varepsilon) = [\varepsilon - \kappa^2/2 - \Sigma(\kappa, \varepsilon)]^{-1}. \quad (20)$$

3.2. Disorder-broadened dispersion relation

Information about the relative weight, energy, and life time of excitations dressed by the disordered medium is contained in the spectral function [56]

$$A(\kappa, \varepsilon) = -2 \operatorname{Im} \overline{G}(\kappa, \varepsilon) = \frac{-2 \operatorname{Im} \Sigma(\kappa, \varepsilon)}{(\varepsilon - \kappa^2/2 - \operatorname{Re} \Sigma(\kappa, \varepsilon))^2 + (\operatorname{Im} \Sigma(\kappa, \varepsilon))^2}. \quad (21)$$

The spectral function is positive, $A(\kappa, \varepsilon) \geq 0$ (because the retarded self-energy has a negative imaginary part), and normalized to unity $\int (d\varepsilon/2\pi) A(\kappa, \varepsilon) = 1$. It can thus be seen to represent the probability density for excitations with wave vector κ to have an energy ε . Its trace over momentum states yields the average density of states per unit volume,

$$\int \frac{d^d \kappa}{(2\pi)^d} A(\kappa, \varepsilon) = 2\pi \mathcal{N}(\varepsilon). \quad (22)$$

The spectral function of a free particle, $A_0(\kappa, \varepsilon) = 2\pi \delta(\varepsilon - \kappa^2/2)$, projects onto the energy shell $\kappa^2 = 2\varepsilon$, such that the free density of states reads as usual

$$\mathcal{N}_0(\varepsilon) = \int \frac{d^d \kappa}{(2\pi)^d} \delta(\varepsilon - \kappa^2/2) = \frac{S_d}{(2\pi)^d} (2\varepsilon)^{d/2-1}. \quad (23)$$

Here $S_d = \int d\Omega_d = 2\pi^{d/2}/\Gamma(d/2)$ denotes the surface of the unit sphere, with the Euler gamma function $\Gamma(x)$.

Whenever the corrections due to disorder are finite but small, $A(\kappa, \varepsilon)$ as a function of ε at fixed κ is strongly peaked around the energy ε_κ defined as a zero of the real dispersion relation $\varepsilon_\kappa - \kappa^2/2 - \operatorname{Re} \Sigma(\kappa, \varepsilon_\kappa) = 0$. A Taylor expansion to lowest order around this point, $\varepsilon - \kappa^2/2 - \operatorname{Re} \Sigma(\kappa, \varepsilon) = (\varepsilon - \varepsilon_\kappa) Z(\kappa)^{-1}$, defines the so-called renormalization constant $Z(\kappa)^{-1} = 1 - \partial_\varepsilon \operatorname{Re} \Sigma(\kappa, \varepsilon)|_{\varepsilon=\varepsilon_\kappa}$. This brings the spectral function into Lorentzian form,

$$A(\kappa, \varepsilon) = Z(\kappa) \frac{\gamma_s}{(\varepsilon - \varepsilon_\kappa)^2 + \gamma_s^2/4}. \quad (24)$$

The mode $|\kappa\rangle$ now represents an excitation with spectral weight $Z(\kappa)$ at energy ε_κ , and with a finite spectral width or elastic scattering rate

$$\gamma_s = -2Z(\kappa) \operatorname{Im} \Sigma(\kappa, \varepsilon_\kappa). \quad (25)$$

This mode describes an atom that is dressed by the speckle fluctuations and scattered into a different mode $|\kappa'\rangle$ on average after a time $\tau_s = 1/\gamma_s$.

Equivalently, one can determine the wave vector $\kappa(\varepsilon)$ corresponding to a given energy ε as the solution to the complex dispersion relation $\varepsilon - \kappa_\varepsilon^2/2 - \Sigma(\kappa_\varepsilon, \varepsilon) = 0$. This is the standard approach in optics [47] and atom optics [57]. Determining the effective dispersion relation of matter waves in disordered speckle potentials is thus reduced to calculating the self-energy.

3.3. The weak scattering approximation

The self-energy defined by the Dyson equation (19) can be expanded as a power series

$$\Sigma = \sum_{n \geq 2} \Sigma_n, \quad (26)$$

where each term Σ_n is the sum of all those irreducible diagrams that contain products of n field correlation functions (4).

For a weakly disordered system, the self-energy can be calculated analytically because only the first contribution Σ_2 needs to be computed. Indeed, the detailed analysis in appendix

Appendix A shows that the ratio of two consecutive terms Σ_n and Σ_{n+1} is proportional to the effective scattering parameter $g = \eta/\kappa$. If the effective scattering is small, $g \ll 1$, the series expansion for Σ can be truncated after the first diagram because the effective medium deviates only slightly from free space. Therefore

$$\Sigma \approx \Sigma_2, \quad (27)$$

which is known as the weak scattering or Born approximation. In terms of the atomic kinetic energy, the weak scattering condition reads $\varepsilon = E/E_\zeta = \kappa^2/2 \gg \eta^2$ or

$$\Delta \equiv \frac{\eta^2}{\varepsilon} = \frac{V_L^2}{EE_\zeta} \ll 1. \quad (28)$$

The weak scattering condition $\Delta \ll 1$ determines the range of validity for the diagrammatic perturbation theory. It can be given a simple physical interpretation by using a semiclassical approximation. The propagation of an incoming plane atomic wave in a speckle potential can in principle be computed using the Feynman path integral. If one assumes that the speckle potential is sufficiently weak, the so-called thin phase grating approximation [58] can be used. There, the classical trajectories $\mathbf{r}_c(t)$ are unaffected by the potential (i.e. remain straight lines), and the additional phase accumulated along each trajectory is simply $\int V(\mathbf{r}_c(t))dt/\hbar$. Along a path with length ζ , the typical accumulated phase will be $V_L\zeta/\hbar v = \sqrt{\Delta}/2$. The weak scattering condition $\Delta \ll 1$ is thus equivalent to the requirement that the accumulated phase be small, i.e. to the applicability condition of the thin phase grating approximation. The atomic wave is then only slightly distorted and scattered after traveling a distance ζ , which also implies that the scattering mean free path is larger than ζ .

Equivalently, the weak scattering condition (28) corresponds to a small quantum reflection probability for a particle that is scattered by a 1D potential barrier with height V_L and linear size ζ . To see this, two cases may be distinguished:

(1) When the potential fluctuations exceed the correlation energy ($V_L > E_\zeta$ or equivalently $\eta > 1$) the weak scattering condition $\Delta \ll 1$ implies $E \gg V_L$ or equivalently $\varepsilon \gg \eta$: the atom flies well above the potential fluctuations. The standard quantum reflection coefficient [59], in our reduced notations

$$R = \left[1 + \frac{4(\varepsilon - \eta)}{\Delta \sin^2(2\sqrt{\varepsilon - \eta})} \right]^{-1} \quad (29)$$

then is indeed small, $R \ll 1$, since the oscillating term is bounded, $|\sin(x)/x| \leq 1$ with $x = 2\sqrt{\varepsilon - \eta}$. This case describes the regime of classical atomic motion.

(2) In the opposite regime of small potential fluctuations ($V_L < E_\zeta$ or equivalently $\eta < 1$) the weak scattering condition can of course also be realized with a fast atom, again without quantum corrections to the classical transport. More interestingly, the weak scattering condition can be met even in the case $E < V_L$, i.e. even when the atomic energy lies *below* the average potential height. The weak scattering regime then is realized if $E \ll E_\zeta$ where the large atomic de Broglie wave length $\lambda_{dB} \gg \zeta$ averages out the short-scale fluctuations and makes the effective disorder weak. In terms of the reflection coefficient (29), this corresponds to the case $\varepsilon < \eta$ and $|\sinh(x)/x| \approx 1$ with $\Delta \ll 1$. We will see below that this is the regime where quantum corrections to classical transport become important.

Finally, the weak scattering condition (28) can be rewritten as

$$E \gg E_\Delta = V_L^2/E_\zeta. \quad (30)$$

Weak-scattering perturbation theory is valid for atoms with a sufficiently high kinetic energy compared to the characteristic energy E_Δ . We will see in section 5.4 that, in $d = 3$ dimensions, E_Δ essentially is the mobility edge [60] which separates extended states with $E > E_\Delta$ from localized states with $E < E_\Delta$.

3.4. Scattering mean free path

Within the weak scattering approximation, the scattering mean free path, a central quantity characterizing the disorder, can be calculated analytically from the microscopic parameters as follows. The relevant self-energy contribution in the Born approximation (27) is given by the momentum convolution of the potential correlation function \mathcal{P}_d with the free Green function G_0 (as detailed in Appendix A):

$$\Sigma_2(\kappa, \varepsilon) = \eta^2 \int \frac{d^d \kappa_1}{(2\pi)^d} \mathcal{P}_d(\kappa - \kappa_1) G_0(\kappa_1, \varepsilon), \quad (31)$$

To lowest order in $\Delta = \eta^2/\varepsilon$ the self-energy can be taken on-shell, $\Sigma_\kappa = \Sigma_2(\kappa, \varepsilon_\kappa)$ with $\varepsilon_\kappa = \kappa^2/2$. For the same reason, the renormalization constant can be approximated by $Z(\kappa) \approx 1$ such that $\gamma_s = -2 \text{Im} \Sigma_\kappa$. Reverting to dimensionfull quantities, the scattering rate defines the elastic scattering mean free path $\ell_s/\zeta = \kappa/\gamma_s$ for a quasi-monochromatic wave packet centered around the momentum $k = \kappa/\zeta$:

$$\frac{\zeta}{\ell_s} = -\frac{2 \text{Im} \Sigma_\kappa}{k\zeta}. \quad (32)$$

The scattering mean free path defines the distance over which a particle travels on average without being scattered. The population of the wave packet decays over the distance r by the factor e^{-r/ℓ_s} , analogously to Beer's law in optics [47]. Consistently with the weak disorder condition $|\Sigma_\kappa| \ll \varepsilon$, we have $\gamma_s/2 \ll \varepsilon$ and equivalently:

$$k\ell_s \gg 1. \quad (33)$$

Note that the scattering mean free path in the Born approximation is inversely proportional to Δ and thus to V_L^2 such that it does not depend on the sign of the laser detuning δ_L .

Taking the imaginary part of equation (31) with the help of $\text{Im} G_0(\kappa, \varepsilon) = -\pi \delta(\varepsilon - \kappa^2/2)$ gives the inverse scattering mean free path (32) in the form

$$\frac{1}{k\ell_s} = \Delta \left(\frac{k\zeta}{2\pi} \right)^{d-2} \int \frac{d\Omega_d}{4\pi} \mathcal{P}_d(k\zeta, \theta). \quad (34)$$

Here, $\mathcal{P}_d(\kappa, \theta) = \mathcal{P}_d(2\kappa|\sin \frac{\theta}{2}|)$ denotes the angular correlation function as a function of the scattering angle θ between κ and κ_1 at fixed on-shell momenta $\kappa = \kappa_1 = k\zeta$. The d -dimensional angular integration measure is $d\Omega_2 = d\theta$ (integration range from 0 to 2π) and $d\Omega_3 = 2\pi \sin \theta d\theta$ (integration range from 0 to π).

3.4.1. 2D speckle The 2D Fourier transform of the potential fluctuation correlation (14a) is a convolution of two identical disks:

$$\mathcal{P}_2(\kappa) = 8 \left[\arccos \frac{\kappa}{2} - \frac{\kappa}{2} \sqrt{1 - \left(\frac{\kappa}{2} \right)^2} \right] \Theta(2 - \kappa). \quad (35)$$

In the angular correlation function $\mathcal{P}_2(2\kappa|\sin \frac{\theta}{2}|)$, the Heaviside function $\Theta(1 - \kappa|\sin \frac{\theta}{2}|)$ restricts the scattering angle to $|\sin \frac{\theta}{2}| < 1/\kappa$. When $\kappa \leq 1$, this condition is always fulfilled, and all angles are possible. When $\kappa > 1$, the scattering direction is restricted to a maximum scattering angle $|\theta| \leq \theta_m = 2 \arcsin(1/\kappa)$: as κ grows, the differential scattering cross section is increasingly peaked in the forward direction. This is illustrated by figure 2(a), a polar plot of the 2D phase function

$$f_2(\kappa, \theta) = \frac{\mathcal{P}_2(\kappa, \theta)}{\int d\theta \mathcal{P}_2(\kappa, \theta)}. \quad (36)$$

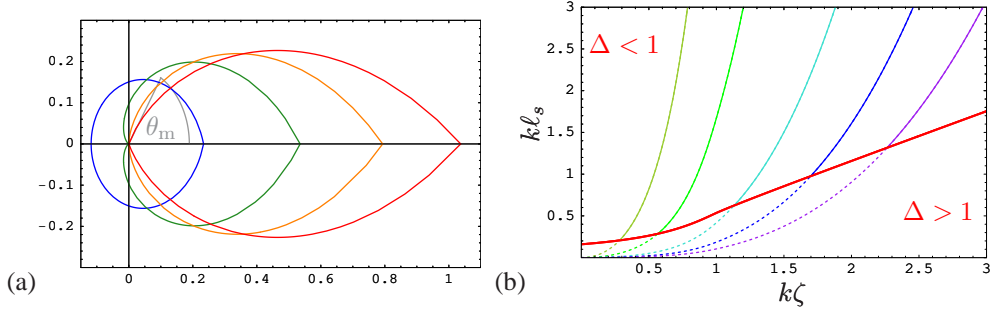


Figure 2. 2D: (a) Phase function (36) for atomic wave vectors $k\zeta = 0.4, 1.0, 1.4, 1.8$ (from left to right: blue, green, orange, red) in units of the speckle correlation length $\zeta = 1/\alpha k_L$. Scattering is nearly isotropic for slow atoms $k\zeta \ll 1$. For fast atoms $k\zeta \gg 1$, scattering is strongly peaked in the forward direction, with a maximal deviation $\theta_m \approx 2/k\zeta$. (b) Disorder parameter $k\ell_s$ as a function of the reduced matter wave number $k\zeta$ for different disorder strengths $\eta = V_L/E_\zeta = 0.2, 0.4, 0.8, 1.2, 1.6$ (thin curves from left to right). The thick red line, connecting points of $k\ell_s$ where $\Delta = 1$, indicates the limit of validity of the weak scattering condition.

For fast atoms $\kappa \gg 1$, the differential scattering cross section is strongly peaked in the forward direction which clearly reveals the anisotropic nature of the scattering process. In this case, $\theta_m \approx 2/\kappa \ll 1$. For slow atoms $\kappa \ll 1$, the differential scattering cross section becomes isotropic. In this case, the correlation function $\mathcal{P}_2(\rho)$ can be approximated by a delta function, i.e. a constant Fourier transform $\mathcal{P}_2(\kappa) \approx 4\pi$. Hence, the angular dependence is lost for $\kappa \ll 1$ and already the first scattering event randomizes the direction of scattering. This isotropic scattering limit, obtained for $\lambda_{dB} \gg \zeta$, corresponds to the s -wave scattering limit in scattering theory.

Using the angular correlation $\mathcal{P}_2(2\kappa|\sin \frac{\theta}{2}|)$ of (35) in (34), it is possible to calculate the scattering mean free path. For $\kappa = 1$, we can do the integral exactly and obtain

$$k\ell_s = \frac{\pi}{2(\pi^2 - 4)\eta^2}, \quad k\zeta = 1. \quad (37)$$

We recall that $\zeta = (\alpha k_L)^{-1}$ is the 2D speckle correlation length and $\eta = V_L/E_\zeta$ the reduced potential strength. It is also possible to obtain analytic results in the limiting cases $\kappa \gg 1$ and $\kappa \ll 1$ where the approximations $\sin x \approx x$ and $\arccos x - x\sqrt{1-x^2} \approx \frac{\pi}{2}$, respectively, can be made:

$$k\ell_s \approx \frac{(k\zeta)^2}{4\pi\eta^2}, \quad k\zeta \ll 1, \quad (38a)$$

$$k\ell_s \approx \frac{3\pi(k\zeta)^3}{32\eta^2}, \quad k\zeta \gg 1. \quad (38b)$$

The condition $\Delta \leq 1$ implies the bound $k\ell_s \geq 1/(2\pi)$, such that weak scattering $\Delta \ll 1$ indeed describes weak disorder $k\ell_s \gg 1$, even at very low momenta. At higher momenta (cf. (38b)), weak scattering $\Delta \leq 1$ implies the bound $\ell_s \geq \frac{3\pi}{16}\zeta$, which agrees with the intuitive expectation that the scattering mean free path cannot be considerably shorter than the 2D speckle correlation length ζ itself. Figure 2(b) shows a plot of $k\ell_s$ as a function of $k\zeta$ obtained by numerical integration of (34). The boundary $\Delta = 1$ indicates the limit of validity of the weak scattering approximation.

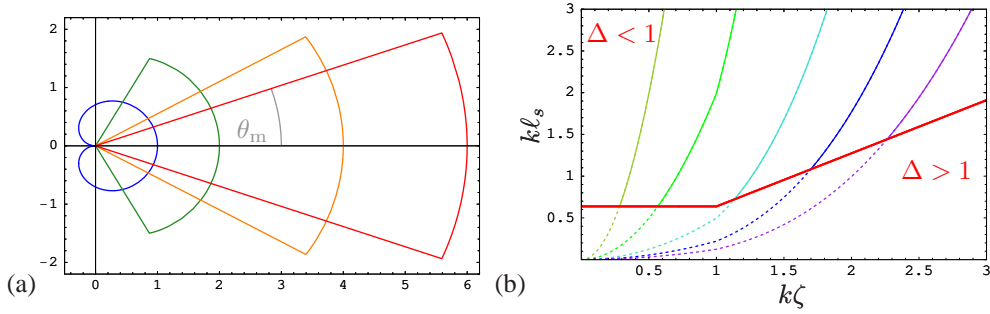


Figure 3. 3D: (a) Effective phase function (40) for atomic wave vectors $k\zeta = 1.0, 2.0, 4.0, 6.0$ (from left to right) in units of the speckle correlation length $\zeta = 1/k_L$, equivalent to velocity in units of recoil velocity, $k\zeta \equiv v/v_R$. All plots with $k\zeta \leq 1$ are identical. When $k\zeta \gg 1$, the phase function is strongly anisotropic and displays the maximum scattering angle $\theta_m \approx 2/k\zeta$. (b) Disorder parameter $k\ell_s$ as a function of the reduced matter wave number $k\zeta$ for disorder strengths $\eta = V_L/E_\zeta = 0.2, 0.4, 0.8, 1.2, 1.6$ (thin curves from left to right). The thick red line connects all points of $k\ell_s$ where $\Delta = 1$, indicating the limit of validity of the weak scattering condition.

3.4.2. 3D speckle In three dimensions, we consider a speckle pattern inside an ergodic cavity. In this case the 3D Fourier transform of the fluctuation correlation function (14b) is a convolution of two identical spherical shells such that

$$\mathcal{P}_3(\kappa) = \frac{\pi^2}{\kappa} \Theta(2 - \kappa). \quad (39)$$

Since $\mathcal{P}_3(\kappa, \theta) = \mathcal{P}_3(2\kappa \sin \frac{\theta}{2})$ diverges in the forward direction $\theta \rightarrow 0$, we plot in figure 3(a) the effective phase function including the angular Jacobian,

$$f_3(\kappa, \theta) = \frac{\sin \theta \mathcal{P}_3(\kappa, \theta)}{\int d\Omega_3 \mathcal{P}_3(\kappa, \theta)}. \quad (40)$$

As for the 2D case, the plot shows bounded scattering $|\theta| \leq \theta_m$ for fast atoms $\kappa > 1$ and unrestricted scattering for slow atoms $\kappa \leq 1$; exact backscattering $\theta = \pi$ appears suppressed due to the angular Jacobian. The inverse elastic mean free path (34) for $d = 3$ is given by

$$\frac{1}{k\ell_s} = \pi \eta^2 [(k\zeta)^{-3} \Theta(k\zeta - 1) + (k\zeta)^{-2} \Theta(1 - k\zeta)], \quad (41)$$

in terms of correlation length $\zeta = k_L^{-1}$ and speckle strength $\eta = V_L/E_\zeta$.

The condition $\Delta \leq 1$ implies the bound $k\ell_s \geq \frac{2}{\pi}$, such that weak scattering $\Delta \ll 1$ indeed describes weak disorder $k\ell_s \gg 1$, even at low momenta. At high momenta, weak scattering $\Delta \leq 1$ implies that $k\ell_s \geq \frac{2}{\pi} k\zeta$, i.e. the lowest achievable scattering mean free path is of the order of the 3D speckle correlation length ζ itself. Figure 3(b) shows a plot of $k\ell_s$ as a function of $k\zeta$ as obtained by (41).

In summary, we have derived the elastic scattering mean free path analytically as a function of all relevant physical parameters. We have taken into account the correlations present in the speckle pattern, using a diagrammatic perturbation theory up to order η^2 in the reduced speckle strength. The validity of the perturbation theory is limited to the regime $\Delta = \eta^2/\varepsilon = V_L^2/EE_\zeta \ll 1$ of not-too-large speckle fluctuations (at fixed atomic energy) and not-too-slow atoms (at fixed speckle strength). Not surprisingly, fast atoms are only weakly deviated by the disordered potential ($k\ell_s \gg 1$). On the other hand, we find that a strongly

scattering disordered medium ($k\ell_s \rightarrow 1$) can be obtained for far-detuned speckle fields of moderate strength and sub-recoil cooled atoms.

4. Diffusive transport

In the present section, we show that the matter-wave dynamics is diffusive on long time scales, and determine the corresponding diffusion constant by using a variant of Vollhardt and Wölfle's diagrammatic perturbation theory [38].

4.1. Density kernels and continuity equation

In the course of its propagation in a disordered potential, the initial matter wave is rapidly turned into a diffuse matter wave invading the entire scattering region. The dynamics of this process is described by the disorder-averaged and forward-propagated probability density to find an atom at position ρ at time $\tau \geq 0$:

$$p(\rho, \tau) = \Theta(\tau) \overline{n(\rho, \tau)} = \Theta(\tau) \text{Tr}\{\overline{\varrho(\tau)} \hat{n}(\rho)\} = \Theta(\tau) \langle \rho | \overline{\varrho(\tau)} | \rho \rangle \quad (42)$$

with $\hat{n}(\rho) = |\rho\rangle\langle\rho|$ the local density operator. Propagating the initial density matrix ϱ_0 in time, one finds $p(\rho, \tau) = \Theta(\tau) \langle \rho | \overline{U(\tau) \varrho_0 U(\tau)^\dagger} | \rho \rangle$. Its Fourier transform $p(\mathbf{q}, \omega) = \int d^d\rho d\tau \exp[i(\omega\tau - \mathbf{q} \cdot \rho)] p(\rho, \tau)$ is given by

$$p(\mathbf{q}, \omega) = \int \frac{d^d\kappa}{(2\pi)^d} \varrho_0(\kappa, \mathbf{q}) \Phi_0(\kappa, \mathbf{q}, \omega), \quad (43)$$

where all information about the initial density distribution is contained in $\varrho_0(\kappa, \mathbf{q}) = \langle \kappa_+ | \varrho_0 | \kappa_- \rangle$ with $\kappa_\pm = \kappa \pm \mathbf{q}/2$. The subsequent propagation is determined by the density propagation kernel

$$\Phi_0(\kappa, \mathbf{q}, \omega) = \int \frac{d^d\kappa'}{(2\pi)^d} \int \frac{d\varepsilon}{2\pi} \Phi(\kappa, \kappa', \mathbf{q}, \varepsilon, \omega) \quad (44)$$

defined in terms of the intensity propagator

$$\Phi(\kappa, \kappa', \mathbf{q}, \varepsilon, \omega) = \overline{\langle \kappa'_+ | G(\varepsilon_+) | \kappa_+ \rangle \langle \kappa_- | G^\dagger(\varepsilon_-) | \kappa'_- \rangle}. \quad (45)$$

Here, $G(\varepsilon_+)$ is the full retarded propagator (15) at energy $\varepsilon_+ = \varepsilon + \omega/2$, and $G^\dagger(\varepsilon_-)$ the full advanced propagator at energy $\varepsilon_- = \varepsilon - \omega/2$. Note that the ensemble average is done after taking their product which means that all correlations between different amplitudes are included. In solid-state physics, this kernel is also known as the “particle-hole” propagator because both a retarded and an advanced Green's function appear.

The average local current density is the expectation value $\hat{j}(\rho, \tau) = \Theta(\tau) \text{Tr}\{\overline{\varrho(\tau)} \hat{j}(\rho)\}$ of the usual current density operator [21] $\hat{j}(\rho) = \frac{1}{2} [\hat{\mathbf{p}} \hat{n}(\rho) + \hat{n}(\rho) \hat{\mathbf{p}}]$. Again going into Fourier components, it reads

$$\hat{j}(\mathbf{q}, \omega) = \int \frac{d^d\kappa}{(2\pi)^d} \varrho_0(\kappa, \mathbf{q}) \Phi_1(\kappa, \mathbf{q}, \omega), \quad (46)$$

which is the analog of (44), i.e. the convolution of the initial distribution with the current kernel

$$\Phi_1(\kappa, \mathbf{q}, \omega) = \int \frac{d^d\kappa'}{(2\pi)^d} \int \frac{d\varepsilon}{2\pi} \kappa' \Phi(\kappa, \kappa', \mathbf{q}, \varepsilon, \omega) \quad (47)$$

that transforms indeed like a vector.

Any Hamiltonian of the form $H = \hat{\mathbf{p}}^2/2m + V(\hat{\mathbf{r}})$ leads to a so-called *continuity equation* that describes the local conservation of the probability density [21]. The only difference with the standard continuity equation in our case comes from the ensemble average that requires to impose forward-time propagation with the Heaviside distribution $\Theta(t)$. The corresponding continuity equation

$$\partial_\tau p(\boldsymbol{\rho}, \tau) + \nabla \cdot \mathbf{j}(\boldsymbol{\rho}, \tau) = \delta(\tau)p(\boldsymbol{\rho}, 0) \quad (48)$$

features the initial condition on the right side. This conservation equation is of course valid for any initial distribution; in terms of the kernels (44) and (47), it takes a very simple form:

$$-i\omega\Phi_0(\boldsymbol{\kappa}, \mathbf{q}, \omega) + i\mathbf{q} \cdot \boldsymbol{\Phi}_1(\boldsymbol{\kappa}, \mathbf{q}, \omega) = 1. \quad (49)$$

This exact relation between the intensity and current kernel does not rely on an expansion for small \mathbf{q} or ω (in contrast to the approximate equation used by Vollhardt and Wölfle and the quantum transport literature.) This is as far as general kinematic definitions can take us. We now have to specify the dynamics, i.e. the equation of motion obeyed by the intensity propagator (45).

4.2. Bethe-Salpeter equation, linear response and diffusion equation

The momentum matrix elements (45) define a four-point operator $\Phi(\varepsilon, \omega) = \overline{G(\varepsilon_+) \otimes G^\dagger(\varepsilon_-)}$ that obeys a Bethe-Salpeter equation:

$$\Phi(\varepsilon, \omega) = [\overline{G(\varepsilon_+) \otimes G^\dagger(\varepsilon_-)}] + [\overline{G(\varepsilon_+) \otimes G^\dagger(\varepsilon_-)}] U(\varepsilon, \omega) \Phi(\varepsilon, \omega). \quad (50)$$

The first term on the right-hand side represents the intensity propagation in the effective medium with uncorrelated average propagators (20). All correlated scattering events are described by the irreducible intensity vertex U . The Bethe-Salpeter equation actually defines U , much in the same way that the Dyson equation (19) defines the self-energy Σ .

Starting from this Bethe-Salpeter equation, the quantum kinetic theory described in Appendix B permits to calculate the current kernel (47) as function of the density kernel (44):

$$i\mathbf{q} \cdot \boldsymbol{\Phi}_1(\boldsymbol{\kappa}, \mathbf{q}, \omega) = \frac{q^2 \kappa^2 \tau(\kappa)}{d} \Phi_0(\boldsymbol{\kappa}, \mathbf{q}, \omega) + i\tau(\kappa) \mathbf{q} \cdot \boldsymbol{\kappa}. \quad (51)$$

This expression is valid in the linear-response regime and for large distances and long times, $q\ell_s \ll 1$ and $\omega\tau_s \ll 1$. It features the transport time $\tau(\kappa)$ given by

$$\frac{1}{\tau(\kappa)} = \int \frac{d\varepsilon}{2\pi} \frac{A(\kappa, \varepsilon)}{2\pi\mathcal{N}(\varepsilon)} \int \frac{d^d\kappa' d^d\kappa''}{(2\pi)^{2d}} A(\kappa', \varepsilon) A(\kappa'', \varepsilon) (1 - \hat{\kappa}' \cdot \hat{\kappa}'') U(\kappa'', \kappa', \varepsilon). \quad (52)$$

The spectral function $A(\kappa, \varepsilon)$ has been defined in (21), and $\mathcal{N}(\varepsilon)$ is the corresponding density of states. The two coupled equations (49) and (51) are easily solved for the density relaxation kernel (44) in the diffusive regime, i.e. to leading order in q and ω :

$$\Phi_0(\boldsymbol{\kappa}, \mathbf{q}, \omega) = \frac{1}{-i\omega + \mathcal{D}(\kappa)q^2}. \quad (53)$$

Here, the *momentum-dependent* diffusion constant is:

$$\mathcal{D}(\kappa) = \frac{\kappa^2 \tau(\kappa)}{d}. \quad (54)$$

Transformed back to time and position variables, the density relaxation kernel

$$\Phi_0(\boldsymbol{\kappa}, \boldsymbol{\rho}, \tau) = \frac{1}{(4\pi\mathcal{D}(\kappa)\tau)^{d/2}} \exp\left[-\frac{\boldsymbol{\rho}^2}{4\mathcal{D}(\kappa)\tau}\right] \quad (55)$$

takes indeed the well-known Gaussian form that obeys the diffusion equation for a unit source term:

$$[\partial_\tau - \mathcal{D}(\kappa)\nabla^2]\Phi_0(\boldsymbol{\kappa}, \boldsymbol{\rho}, \tau) = \delta(\boldsymbol{\rho})\delta(\tau). \quad (56)$$

4.3. Boltzmann transport of matter waves

The irreducible vertex operator U entering equation (52) describes the average scattering of the local probability density. U can be expanded in a power series just like the self-energy (26):

$$U = \sum_{n \geq 2} U_n, \quad (57)$$

U_n is proportional to the speckle strength η to the power n , and contains all irreducible contributions with n field correlations and at least one correlation between the retarded and advanced amplitude. Due to the non-Gaussian character of intensity correlations, its diagrammatic representation (shown in Appendix C) differs from the standard form for Gaussian potentials.

Generally, U cannot be calculated exactly since correlations of arbitrary order are involved, and one has to resort to an approximation. In the Boltzmann approximation (also known as the independent scattering approximation), the infinite series (57) is truncated after the lowest-order contribution U_2 such that

$$U(\boldsymbol{\kappa}, \boldsymbol{\kappa}', \varepsilon) \approx U_B(\boldsymbol{\kappa}, \boldsymbol{\kappa}', \varepsilon) = \eta^2 \mathcal{P}_d(\boldsymbol{\kappa} - \boldsymbol{\kappa}'). \quad (58)$$

The corresponding Boltzmann intensity (53) describes multiple scattering as a sequence of scattering events where both retarded and advanced amplitudes travel along the same path. In other words, all interference effects have been discarded. This approximation thus provides a microscopic justification of the classical Boltzmann-Lorentz transport theory for non-interacting particles in the presence of quenched disorder that has been successfully applied to a large number of physical systems, ranging from the Drude transport theory of electrons in metals [26] to the radiative transfer equation in optics [27, 28].

The Boltzmann approximation (58) for the intensity vertex is very similar to the weak scattering approximation (27) for the self-energy. In fact, these two approximations are intimately linked by the local conservation of the probability density as expressed by the continuity equation (49) (which is guaranteed by a Ward identity (B.4) in the diagrammatic perturbation theory, see Appendix B).

In the present case, inserting the vertex (58) into the general expressions (52) and (54) defines a dimensionfull Boltzmann transport mean free path ℓ_B according to

$$\mathcal{D}_B = \frac{\kappa^2 \tau_B(\kappa)}{d} = \frac{m D_B}{\hbar} = \frac{k \ell_B}{d}. \quad (59)$$

To zeroth order in $\Delta = \eta^2/\varepsilon$, the spectral functions in (52) reduce to the on-shell projector $A_0(\kappa, \varepsilon) = 2\pi\delta(\varepsilon - \kappa^2/2)$ such that

$$\frac{1}{k\ell_B} = \Delta \left(\frac{k\zeta}{2\pi} \right)^{d-2} \int \frac{d\Omega_d}{4\pi} (1 - \cos\theta) \mathcal{P}_d(k\zeta, \theta), \quad (60)$$

where $\mathcal{P}_d(\kappa, \theta) = \mathcal{P}_d(2\kappa|\sin\frac{\theta}{2}|)$ is the angular potential correlation function with θ the angle between $\boldsymbol{\kappa}$ and $\boldsymbol{\kappa}'$ at on-shell momenta $\kappa = \kappa' = k\zeta$. The transport mean-free path is the average distance required to completely erase the memory of the initial direction of propagation. It is related to the scattering mean free path (34) through

$$\frac{\ell_s}{\ell_B} = 1 - \langle \cos\theta \rangle = 1 - \int d\Omega_d \cos\theta f_d(k\zeta, \theta), \quad (61)$$

where the cosine of the scattering angle is averaged over the phase function (36) or (40). This term is known as the *anisotropy factor* of the scattering process. For fully isotropic scattering, it is of course zero, and $\ell_B = \ell_s$. But for strongly anisotropic scattering, $\langle \cos\theta \rangle$ can take a

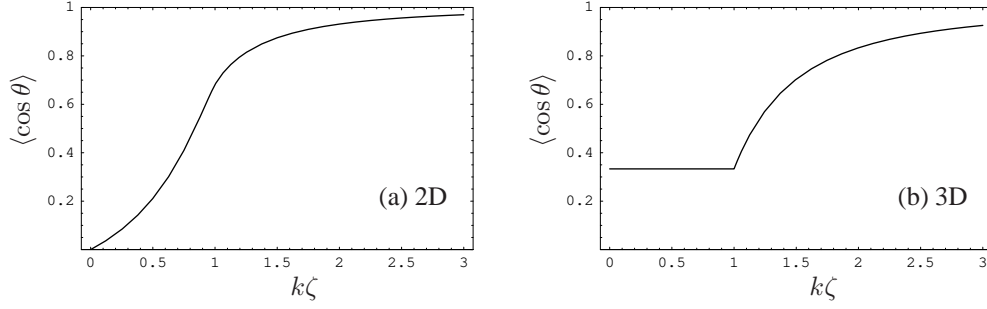


Figure 4. Plot of the anisotropy factor as a function of the reduced atomic wave number $k\zeta$. (a) 2D ($\zeta = 1/\alpha k_L$): For small wave numbers ($k\zeta \rightarrow 0$) the anisotropy decreases ($\langle \cos \theta \rangle \rightarrow 0$) and the scattering becomes isotropic ($\ell_B \rightarrow \ell_s$). For large wave numbers ($k\zeta \gg 1$), the anisotropy becomes more pronounced ($\langle \cos \theta \rangle \rightarrow 1$). (b) 3D ($\zeta = 1/k_L$): Large wave numbers show strong scattering anisotropy. But even for small wave numbers, scattering is never really isotropic, $\langle \cos \theta \rangle = \frac{1}{3}$ for all $k\zeta \leq 1$, as already indicated by the anisotropic phase function plotted in figure 3(a).

value close to 1. In this case, a large number of scattering events is necessary to deviate the particle completely, $\ell_B \gg \ell_s$. In the language of diagrammatic quantum transport theory, the anisotropy factor (61) is due to *vertex corrections* [56] that are obtained by summing the entire series known as *ladder diagrams*; see Appendix C for details.

4.3.1. 2D-speckle In the limiting cases where analytical solutions are found (cf. (37) and (38a)),

$$\ell_B \approx \ell_s, \quad k\zeta \ll 1, \quad (62a)$$

$$\ell_B = \frac{\pi^2 - 4}{\pi^2 - 8} \ell_s, \quad k\zeta = 1 \quad (62b)$$

$$\ell_B \approx \frac{15}{4} (k\zeta)^2 \ell_s, \quad k\zeta \gg 1. \quad (62c)$$

A plot of the 2D anisotropy factor $\langle \cos \theta \rangle$ (computed numerically) as a function of $k\zeta$ is shown in figure 4.3.1. For small wave numbers $k\zeta \rightarrow 0$, one has $\langle \cos \theta \rangle \rightarrow 0$ and $\ell_B \rightarrow \ell_s$: the scattering is isotropic. When $k\zeta \gg 1$, the ratio ℓ_B/ℓ_s scales as $(k\zeta)^2$. This can be easily understood because the phase function limits the angular integration to $|\theta| \leq \theta_m \sim 1/k\zeta$ such that $1 - \langle \cos \theta \rangle \approx \frac{1}{2} \langle \theta^2 \rangle \propto \theta_m^2$. Thus roughly $(k\zeta)^2$ independent scattering events are needed to fully erase the memory of the initial direction. In other words, the monochromatic laser photons with limited projected wave vectors αk_L which are present in the speckle field can only weakly deviate atoms with large momentum $k \gg \alpha k_L$.

4.3.2. 3D-speckle For the 3D case, the integration of (60) yields the exact result:

$$\frac{1}{k\ell_B} = \frac{2\pi}{3} \eta^2 [(k\zeta)^{-5} \Theta(k\zeta - 1) + (k\zeta)^{-2} \Theta(1 - k\zeta)]. \quad (63)$$

In terms of the scattering mean free path (41) we have

$$\ell_B = \frac{3\ell_s}{2} [(k\zeta)^2 \Theta(k\zeta - 1) + \Theta(1 - k\zeta)]. \quad (64)$$

As one can see in figure 4.3.1, a slight anisotropy $\ell_B = \frac{3}{2}\ell_s$ remains for all $k\zeta \leq 1$, implying $\langle \cos \theta \rangle = \frac{1}{3}$. This is explained by the absence of scattering around the backscattering direction

after multiplying the finite differential cross section by the vanishing angular Jacobian, as already evidenced by the anisotropic phase function plotted in figure 3(a). This residual anisotropy is due to the long range correlations in the optical potential, as exemplified by the divergence of $\mathcal{P}_3(\boldsymbol{\kappa})$, see eq. (39), near $\kappa = 0$. At higher momenta, $k\zeta \geq 1$, the ratio ℓ_B/ℓ_s scales as $(k\zeta)^2$, for the same reason as in 2D.

This closes our study of the classical transport properties of monochromatic matter waves in correlated speckle potentials. Essentially, we have found diffusive dynamics, as expected for particles in a conservative random potential, with a transport mean free path displaying a strong anisotropy for fast atoms, and becoming approximately isotropic for cold enough atoms. In the following, we investigate quantum corrections to classical transport.

5. Coherent multiple scattering

5.1. Quantum corrections to classical transport

Within the Boltzmann approximation, all quantum interference effects are discarded. At first sight this seems reasonable since any such effects could be expected to be suppressed by the ensemble average over all possible realizations of the random potential. This means that the disorder average singles out products of amplitudes and conjugate amplitudes traveling along the same paths in the same direction where no phase differences are present. In the language of electronic quantum transport, these are the “particle-hole contributions”. They are insensitive to dephasing processes and therefore correspond to classical propagation.

It was realized however, that this argument is too simplistic [61] for phase-coherent systems, where interference between amplitudes of different scattering paths can occur. This can be easily understood by considering the return probability to a given point in which case all scattering paths are closed loops. Two waves propagating in opposite directions around any such loop have zero phase difference and interfere constructively (unless a magnetic field for charged particles is applied, or dephasing processes are at work). This constructive two-wave interference enhances the return probability to twice the classically expected value. An enhanced return probability in turn implies a reduced diffusion constant for the onward propagation, an effect known as *weak localization*.

Quantum corrections to the Boltzmann transport picture are accounted for by including the sum of all counter-propagating amplitudes in the irreducible vertex U used in (52): $U = U_B + C$ [38, 53]. The so-called Cooperon contribution C can be expressed in terms of the diffusive intensity kernel (53) using a time-reversal argument for the advanced amplitude as

$$C(\boldsymbol{\kappa}, \boldsymbol{\kappa}', \varepsilon, \omega) = \frac{1 - \langle \cos \theta \rangle}{4\pi\mathcal{N}(\varepsilon)\tau_s^2} \frac{1}{-i\omega + \mathcal{D}_B(\kappa)Q^2}. \quad (65)$$

It is a strongly peaked function around the backscattering direction $\mathbf{Q} = \boldsymbol{\kappa} + \boldsymbol{\kappa}' = 0$. The anisotropy factor $(1 - \langle \cos \theta \rangle)$ can be justified by considering dressed Hikami boxes as explained in Appendix D. Inserting (65) into the general definition (52), one can replace the double integral over $\boldsymbol{\kappa}'$ and $\boldsymbol{\kappa}''$ by a single integral over \mathbf{Q} (with suitable cut-offs for very small and very large momenta, see discussion below) such that the corrected inverse diffusion constant (54) reads

$$\frac{1}{\mathcal{D}^*(\kappa, \omega)} = \frac{1}{\mathcal{D}_B(\kappa)} \left(1 + \frac{1}{\pi\mathcal{N}_0(\varepsilon_\kappa)} \int \frac{d^d Q}{(2\pi)^d} \frac{1}{-i\omega + \mathcal{D}_B(\kappa)Q^2} \right). \quad (66)$$

The interference correction inside the parenthesis is the leading term in an expansion in powers of $1/k\ell_B \leq 1/k\ell_s \ll 1$. For this reason the denominator contains the free density of states $\mathcal{N}_0(\varepsilon)$ instead of the disorder-averaged density of states $\mathcal{N}(\varepsilon)$.

This perturbation theory for the *inverse* diffusion constant $\mathcal{D}^*(\kappa)^{-1} = \mathcal{D}_B(\kappa)^{-1}(1 + \epsilon)$ is only meaningful for a small correction $\epsilon < 1$ such that the resulting diffusion constant is bounded from below as $\mathcal{D}^*(\kappa) > \mathcal{D}_B/2$. Vollhardt and Wölfe [38] have devised a self-consistent resummation of the perturbation series that allows in principle to reach the strong localization threshold $\mathcal{D}^*(\kappa) \rightarrow 0$: one simply has to replace the Boltzmann diffusion constant in the denominator of (66) by the corrected diffusion constant $\mathcal{D}^*(\kappa, \omega)$ itself. This prescription amounts to summing iterated loops of counterpropagating amplitudes. As a net result, weak localization reduces the stationary diffusion constant according to $\mathcal{D}^* = \mathcal{D}_B - \delta\mathcal{D}$, with the quantum correction (see Appendix D for more details):

$$\delta\mathcal{D} = \frac{1}{\pi\mathcal{N}_0(\varepsilon_\kappa)} \int \frac{d^d Q}{(2\pi)^d} \frac{1}{Q^2 + 1/\lambda_*^2}. \quad (67)$$

Here, the small- Q divergence of the soft mode under the integral is cut off by the real quantity $\lambda_* := \lim_{\omega \rightarrow 0} [-i\omega/\mathcal{D}^*(\omega)]^{-1/2}$. The characteristic length $L_* = \zeta\lambda_*$ can encapsulate several effects that limit the interference of amplitudes traveling around large loops of a characteristic size: (i) limited system size L , (ii) finite phase-coherence length L_ϕ , and (iii) strong localization on a scale ξ_{loc} such that in general

$$\frac{1}{L_*^2} = \frac{1}{L^2} + \frac{1}{L_\phi^2} + \frac{1}{\xi_{\text{loc}}^2}. \quad (68)$$

This length has been found to monitor correctly the behavior of the diffusion constant in bulk media ($L \rightarrow \infty$) in the presence of phase-breaking mechanisms close to the strong localization threshold [62]. The interesting physics associated with these effects in the weak localization regime and at the threshold to strong localization will be discussed in the following subsections.

The integral (67) also diverges in the UV limit $Q \rightarrow \infty$ because we took the spectral functions inside the double integral (52) at $Q = 0$. This divergence can thus be remedied by introducing an ultraviolet cutoff $Q_{\text{max}} = \zeta/\ell_c$ given a priori by the overlap of the disorder-broadened spectral functions, i.e. $\ell_c = \ell_s$, as discussed by van Tiggelen [31]. We have chosen this cut-off in our previous publication [39]. However, in the present case of correlated scattering, loops of counterpropagating amplitudes can only be closed on the larger length scale $\ell_B \geq \ell_s$. Therefore $\ell_c = \ell_B$ seems more adequate. In particular, this choice is consistent with the diffusion approximation and provides particularly simple expressions in the following. There is no need to renormalize this microscopic cutoff length self-consistently as the diffusion constant, i.e. to replace ℓ_B by ℓ^* , since on the short time scale $\omega^{-1} \approx \tau_B$ during which the matter wave is scattered around a small closed loop, the weak localization corrections (66) to classical scattering are negligible. The precise choice for the small-scale cutoff ℓ_c in any case can only shift the non-universal, perturbative prediction of the onset, but does not affect universal predictions like critical exponents at the transition to the strongly localized regime; see section 5.4 below.

5.2. Weak localization

First we will study weak localization for a monochromatic diffusing matter wave with wave number k (determined by the cooling technology at hand) inside a speckle field of fixed size L , as a function of the laser intensity I_L and the detuning δ_L as externally controllable parameters in the experiment.

For the observation of the weak localization correction a *coherent* diffusive process must be established inside a large enough scattering region. This means that the total size of the scattering medium must be large enough to admit diffusion in the first place, $L > \ell_B$. And

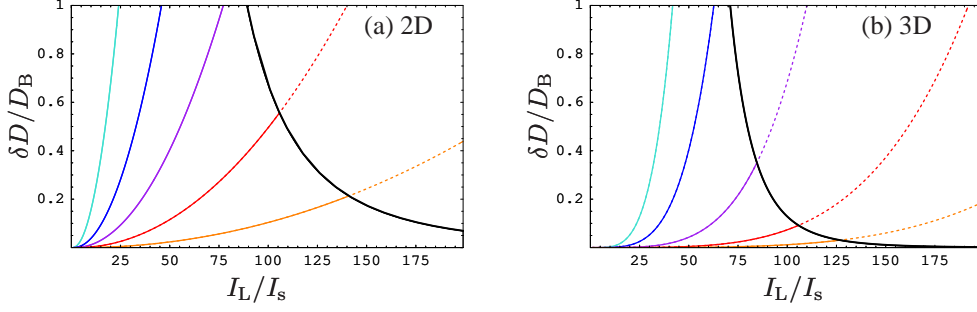


Figure 5. Weak localization correction $\delta D/D_B$ as a function of the reduced intensity I_L/I_s in a speckle field of size $L = 2$ cm.

(a) 2D: matter wave numbers $k\zeta \in \{0.8, 1.0, 1.2, 1.5, 2.0\}$ (from left to right) with laser detuning $\delta_L = 10^6 \Gamma$.

(b) 3D: matter wave numbers $k\zeta \in \{0.6, 0.9, 1.2, 1.5, 1.8\}$ (from left to right) with laser detuning $\delta_L = 10^4 \Gamma$.

The weak scattering condition $\Delta < 1$ is valid to the left of the thick black line.

phase-breaking events must occur at a small enough rate $\gamma_\phi = 1/\tau_\phi < \gamma_s$. Otherwise, if the phase coherence is immediately destroyed between two consecutive scattering events, the propagation remains entirely classical, and the Boltzmann transport theory of section 4 applies. The *phase coherence length* $L_\phi = \sqrt{D_B \tau_\phi}$ is the scale beyond which phase breaking mechanisms destroy weak localization. Both finite sample size and finite phase coherence are taken into account by using the characteristic infrared length (68) in the weak localization regime ($\xi_{\text{loc}} \rightarrow \infty$) as

$$\frac{1}{L_*^2} = \frac{1}{L^2} + \frac{1}{L_\phi^2}. \quad (69)$$

To ensure that interference corrections can be observed experimentally, one has to satisfy both the diffusive and coherent transport condition, $L_* \gg \ell_B$.

For atoms experiencing the light shift (1) inside the speckle field, the phase-breaking mechanism at work is inelastic photon scattering, i. e. absorption and spontaneous reemission of a photon into a different field mode accompanied by a recoil momentum kick for the scattering atom. Thus $\tau_\phi = \tau_i = \gamma_i^{-1}$, with the inelastic scattering rate $\gamma_i \propto V_L/\delta_L$ given by (2). The coherence time can be made arbitrarily large by increasing the detuning δ_L at a fixed potential strength $V_L \propto I_L/\delta_L$. We will show in the following that the phase coherence requirements can be met with reasonable values for relevant experimental parameters.

The 2D weak localization correction (67) relative to the Boltzmann diffusion constant (59) reads in dimensionfull units and in the regime $\ell_c = \ell_B \ll L_*$ given by (69):

$$\frac{\delta D}{D_B} = \frac{2}{\pi} \frac{\ln(L_*/\ell_B)}{k\ell_B}. \quad (70)$$

Noticeable corrections can be expected for strong disorder where $k\ell_B$ is not too large.

Figure 5(a) shows the relative weak localization correction $\delta D/D_B$ as a function of the laser intensity I_L for different initial atomic velocities, at fixed laser detuning $\delta_L = 10^6 \Gamma$ and speckle size $L = 2$ cm. At its limit of validity $\Delta = 1$, our theory predicts that the weak localization correction δD reaches already 20% of the Boltzmann diffusion constant D_B itself for $k\zeta = 2.0$. For a smaller wave number $k\zeta = 1.5$, the value of $\delta D/D_B$ rises to 55%. Since $\zeta = 1/\alpha k_L \gg 1/k_L$, experimental evidence of 2D weak localization requires initial temperatures for the atomic sample well below the recoil temperature. In turn, this

means using a Bose-Einstein condensate as the initial atomic matter wave. As a general rule, the colder the atoms, the larger are the interference corrections.

In 3D, the weak localization correction (67) relative to the Boltzmann diffusion constant (59) reads for $L_* \gg \ell_c = \ell_B$

$$\frac{\delta D}{D_B} = \frac{3}{\pi} \frac{1}{(k\ell_B)^2}. \quad (71)$$

The 3D interference corrections are small in the weak disorder regime $k\ell_s \gg 1$. The relative weak localization correction $\delta D/D_B$ as a function of the laser intensity for a speckle size $L = 2$ cm and detuning $\delta = 10^4 \Gamma$ are shown in figure 5(b). As expected, the largest interference corrections are obtained when $k\zeta \leq 1$, which means initial sub-recoil temperatures. Here again, an experimental study may require a Bose-Einstein condensate as the matter wave source.

5.3. Strong localization: 2D

The 2D interference correction (70) to the diffusion constant diverges with $L_* \rightarrow \infty$ which indicates that a perfectly phase-coherent wave in an infinite disordered 2D system is in fact always localized, as predicted by the single-parameter scaling theory [30]. The corrected diffusion constant vanishes, $D^* \rightarrow 0$, at the threshold determined for $k\ell_B \geq k\ell_s \gg 1$ by

$$\ln(L_*/\ell_B) = \frac{\pi}{2} k\ell_B. \quad (72)$$

This condition defines a curve in (δ_L, I_L) parameter space. In figure 6(a) we plot the corresponding “phase diagram” showing the boundary between the weak and the strong localization regime for different atomic velocities. The curves are almost straight lines because the Boltzmann mean free path ℓ_B in the denominator of (70) scales as $\eta^2 \propto V_L^2$. As a consequence $\delta D/D_B$ scales as $(I_L/\delta_L)^2$, with small corrections from the logarithmic dependence on L_*/ℓ_B . Consequently, the strong localization onset has a linear dependence in the (δ_L, I_L) plane with a slope determined by the atomic wave number k .

For each point on these curves, one can deduce the corresponding values for the multiple scattering parameters. For example, for Rubidium 87 atoms ($m = 1.44 \cdot 10^{-25}$ kg, $\lambda_A = 780$ nm, $I_s = 1.67$ mW/cm², $\Gamma/2\pi = 6$ MHz) at $k\zeta = 1.2$, $L = 2$ cm, $I_L = 77$ I_s, and $\delta_L = 10^6 \Gamma$, we find a scattering mean free path $\ell_s = 0.8 \mu\text{m}$, a transport mean free path $\ell_B = 4.1 \mu\text{m}$ and a phase coherence length $L_\phi \approx 2$ mm. This places the strong localization threshold at $k\ell_s \approx 0.81$. These numbers are of course to be taken with a grain of salt since they are obtained by applying the weak scattering approximation quite close to the limit of its validity (at the transition point $\Delta \approx 0.83$).

In the strong localization regime, extended atomic wavefunctions become exponentially localized as a function of the distance, and the corresponding localization length ξ_{loc} enters as a new length scale. In a bulk system $L \rightarrow \infty$ the characteristic length (68) then reads $1/L_*^2 = 1/L_\phi^2 + 1/\xi_{\text{loc}}^2$ [62]. Together with equation (72), this determines the 2D localization length ξ_{loc} as function of the atomic wave vector and the other experimentally relevant parameters.

We study in figure 6(b) the characteristic length scales on both sides of the strong localization threshold as a function of the laser intensity I_L for $k\zeta = 1.2$, $L = 2$ cm, $\alpha = 0.1$, and fixed laser detuning $\delta_L = 10^6 \Gamma$. With increasing laser intensity, the phase coherence length L_ϕ (blue dashed curve) decreases since the probability of spontaneous photon scattering increases. The Boltzmann transport mean free path ℓ_B (turquoise dashed curve), a purely local quantity, shows no particular singularity, but the corrected mean-free

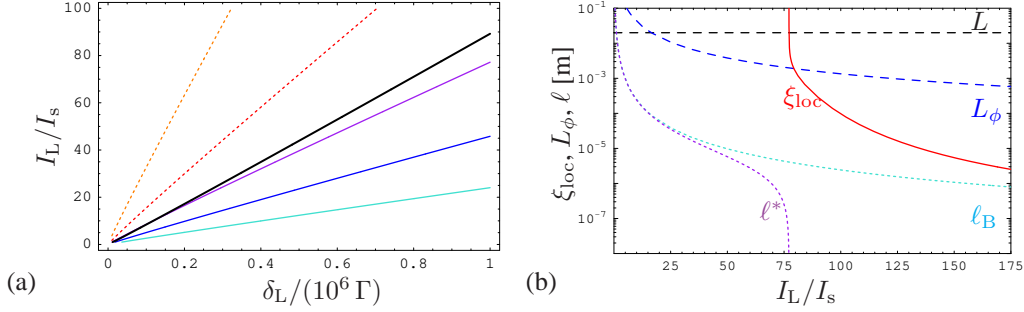


Figure 6. 2D: (a) Strong localization onset defined by $\delta D = D_B$ in (δ_L, I_L) phase space for different atomic wavenumbers $k\zeta \in \{0.8, 1.0, 1.2, 1.5, 2.0\}$ (from right to left) in a speckle field of size $L = 2$ cm. For each value of $k\zeta$, the strong localization regime lies above and to the left of the corresponding line. The red line corresponds to the criterion $\Delta = 1$. Solid curves below can reach the strong localization onset within the weak scattering regime; dotted curves are merely extrapolated.

(b) Logarithmic plot of the Boltzmann transport mean free path ℓ_B , the weak localization corrected transport mean free path ℓ^* , the phase coherence length L_ϕ , and the localization length ξ_{loc} as a function of laser intensity I_L in units of saturation intensity I_s for a fixed atomic wave vector $k\zeta = 1.2$ and detuning $\delta_L = 10^6 \Gamma$ inside a speckle field of $L = 2$ cm. At the strong localization threshold $I_L = 77 I_s$, the corrected transport mean free path $\ell^* = 2mD^*/\hbar k$ vanishes. For higher intensities the matter wave is localized with a finite localization length ξ_{loc} .

path ℓ^* (violet dashed line) plunges to zero together with the corrected diffusion constant $D^* = \hbar k \ell^*/2m$ at the threshold value $I_L = 77 I_s$. This threshold value corresponds precisely to the transition point on the phase boundary in figure 6(a) reached with $L_* = L_\phi = 2$ mm. At the same point, the localization length ξ_{loc} (red full curve) comes down from infinity and tends to the expression derived from (72) in the limit $\xi_{\text{loc}} \ll L_\phi$ of strong localization: $\xi_{\text{loc}} = \ell_B \exp[\frac{\pi}{2} k \ell_B]$.

5.4. Strong localization: 3D

Contrary to the 2D case, the 3D correction (71) remains finite as $L_* \rightarrow \infty$. Therefore, a transition to the strongly localized regime cannot be driven solely by large-scale coherence, but requires strong enough local disorder. This essential difference between the 2D and the 3D case can be traced back to the fact that a random walk in 2D returns to the origin with unit probability, whereas in 3D it escapes with finite probability to infinity [63, 64].

As shown by Vollhardt and Wölfle [65], the self-consistent weak localization prediction (67) allows to calculate the critical exponents of the localization length and the diffusion constant at the Anderson phase transition in an arbitrary dimension $d > 2$. We shall use their findings for $d = 3$. The integral in (67) can be evaluated with an arbitrary UV-cutoff ζ/ℓ_c using the identity $x^2/(1+x^2) = 1 - 1/(1+x^2)$. At the threshold $\delta D = D_B$, it yields a transcendental equation for L_* [21, 65]:

$$\frac{L_*}{\ell_c} \left[1 - \left(\frac{\gamma_0}{\gamma} \right)^2 \right] = \arctan \frac{L_*}{\ell_c}. \quad (73)$$

Here the disorder parameter γ and its critical value γ_0 are defined as

$$\gamma = \frac{1}{k\sqrt{\ell_c \ell_B}}, \quad \gamma_0 = \sqrt{\pi/3}. \quad (74)$$

The ratio γ/γ_0 determines whether (73) admits a solution $L_* > 0$ and thus a finite localization length. The usual graphical solution of $bx = \arctan x$ shows that there is no finite solution for L_* in the diffusive regime of small disorder $\gamma < \gamma_0$. In this case, the matter wave shows truly diffusive dynamics on all scales larger than ℓ_B with finite diffusion constant $D^* > 0$ weakly localized by the correction (71).

In the localized regime $\gamma > \gamma_0$, (73) admits a finite solution $L_* > 0$ that tends critically towards infinity as $\gamma \rightarrow \gamma_0$. Using $\arctan(L_*/\ell_c) \approx \pi/2$, one finds $L_* \sim |\gamma - \gamma_0|^{-\nu}$ with the critical exponent $\nu = 1$. Both the diagrammatic perturbation theory and the scaling theory [33] thus lead to the same critical exponent $\nu = 1$.

Universal quantities like critical exponents are independent of the cut-off ℓ_c , in contrast to the disorder parameter and the critical threshold as defined in (74). The parameter γ simplifies considerably if we identify the cut-off length ℓ_c with the Boltzmann transport mean free path as justified in section 5.1 above. With this choice $\gamma = 1/k\ell_B$, we locate the strong localisation threshold $\gamma_c = \gamma_0$ or $\delta D/D_B = 1$ at the critical disorder strength or critical Ioffe–Regel parameter [31]

$$k\ell_B^c = \sqrt{\frac{3}{\pi}} \approx 0.95. \quad (75)$$

In order to estimate whether this strong localization threshold can be reached with current experimental techniques, we use the perturbative results of section 3 and 4 to calculate the laser intensity and detuning for different atomic momenta. For sufficiently large and phase-coherent systems, $L_* \gg \ell_B$, we have $\delta D/D_B \propto (I_L/\delta_L)^4$. In the (I_L, δ_L) parameter plane, the strong localization threshold $\delta D/D_B = 1$ is thus characterized by the simple linear scaling $I_L \propto \delta_L$. This can be seen in the phase diagram of the 3D strong localization onset for different atomic wave vectors in figure 7(a).

For an atom prepared at recoil momentum $k = 0.9 k_L$, and a realistic detuning $\delta_L = 10^4 \Gamma$, we locate the strong localization threshold at a very reasonable laser intensity $I_L = 63 I_s$. At this point $\ell_s = 0.09 \mu\text{m}$, $\ell_B = 0.13 \mu\text{m}$ and the phase coherence length $L_\phi = 9 \mu\text{m}$. Precisely at the transition point, the corrected transport mean-free path vanishes, $\ell^* = 0$. Since $L_* \gg \ell_B$ the coherent transport condition is well fulfilled. Again these numbers have to be taken with a grain of salt since the underlying perturbative description is bound to break down in the strongly disordered regime.

The self-consistent equation (73) permits to describe the localized regime. Close to the threshold, it reads

$$\frac{L_*}{\ell_B} = \frac{3/2}{3/\pi - (k\ell_B)^2}. \quad (76)$$

Together with (68) this expression determines the 3D localization length ξ_{loc} .

Figure 7(b) shows a logarithmic plot of the relevant length scales on both sides of the localization threshold for a fixed atomic momentum of $k = 0.9 k_L$ as function of the intensity I_L at $\delta = 10^4 \Gamma$. Just as in 2D, the phase coherence length decreases monotonically because spontaneous photon emission is enhanced as the power increases. The strong localization threshold is reached for $I_L = 63 I_s$, where the corrected transport mean free path ℓ^* vanishes together with the diffusion constant. As expected the localization length ξ_{loc} comes down from infinity at the threshold and tends toward its bulk value $\xi_{\text{loc}} = \frac{3}{2}\ell_B/(\frac{3}{\pi} - k^2\ell_B^2)$ given by (76) in the regime $\xi_{\text{loc}} \ll L_\phi, L$.

Often the critical behavior of L_* is stated as a function of the energy which enters in our case the Boltzmann transport mean free path $\ell_B(k)$. For sub-recoil atoms $k\zeta \leq 1$, the disorder

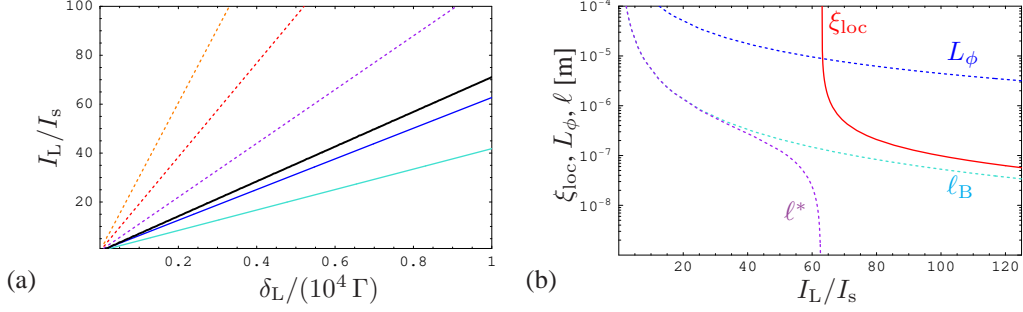


Figure 7. 3D: (a) Strong localization onset defined by $\delta D = D_B$ in (δ_L, I_L) phase space for different atomic wavenumbers $k\zeta \in \{0.6, 0.9, 1.2, 1.5, 1.8\}$ (from right to left) in a speckle field of size $L = 2$ cm. For each value of $k\zeta$, the strong localization regime lies above and to the left of the corresponding line. The red line corresponds to the criterion $\Delta = 1$. Solid curves below can reach the strong localization onset within the weak scattering regime; dotted curves are merely extrapolated.

(b) Logarithmic plot of the Boltzmann transport mean free path ℓ_B , the weak localization corrected transport mean free path ℓ^* , the phase coherence length L_ϕ , and the localization length ξ_{loc} as a function of laser intensity I_L in units of saturation intensity I_s for $k\zeta = 0.9$ and $\delta = 10^4 \Gamma$. At the strong localization threshold $I_L = 63 I_s$, the corrected transport mean free path $\ell^* = 3mD^*/\hbar k$ vanishes. For higher intensities the matter wave is localized with a finite localization length ξ_{loc} .

parameter can be expressed in terms of the energy making use of (30) and (63):

$$\frac{\gamma}{\gamma_0} = \frac{E_c}{E} = \sqrt{\frac{\pi}{3}} \frac{E_\Delta}{E}. \quad (77)$$

where E_c denotes the mobility edge. Up to the non-universal factor $\gamma_0 = \sqrt{\pi/3}$ very close to unity, it is given by the weak-scattering energy scale E_Δ defined in (30). The critical exponent as function of energy is still the same, $L_* \propto (E_c - E)^{-\nu}$ with $\nu = 1$. For above-recoil atoms $k\zeta \geq 1$, the threshold condition $\gamma = \gamma_0$ leads to an energy such that the weak-scattering parameter $\Delta \geq 1$ lies formally beyond its limit of validity; in this regime, our first-order perturbation theory cannot give trustworthy estimates for the mobility edge.

Similarly, we can calculate the critical exponent of the diffusion constant decreasing to zero on the diffusive side $\gamma < \gamma_0$ of the transition, $D^* \propto (\gamma_0 - \gamma)^s \propto (E - E_c)^s$ with the same critical exponent $s = 1$ as predicted by the scaling theory [33]. This is particularly remarkable since the diagrammatic perturbation theory is in principle only valid for weak disorder and a priori cannot describe the strong localization onset. The accurate description of the critical exponents within this theory however can be seen as a strong hint that the quantum interference corrections, which are responsible for weak localization, also remain the dominant contribution for strong localization.

6. Conclusion and Outlook

We have formulated a quantum transport theory for non-interacting matter waves in two- and three-dimensional disordered optical speckle potentials with a finite, and rather large, correlation length ζ . Making use of diagrammatic perturbation theory for weak scattering, we have determined all relevant microscopic transport parameters (scattering mean free path ℓ_s , transport mean free path ℓ_B and Boltzmann diffusion constant D_B) that are necessary to

describe the average diffusion process, as functions of experimentally controllable quantities such as the initial atomic momentum, the laser detuning and the laser intensity.

As a consequence of the speckle correlations we encounter an essential difference compared to the common treatment for Gaussian white noise. The differential single scattering cross section for correlated fluctuations is anisotropic and its degree of anisotropy depends strongly on the initial energy of the matter wave. This is a general property of correlated potentials which has important implications for the small perturbation parameter that determines the limit of the weak scattering regime. Together with the strength of the potential fluctuations V_L , the speckle correlation length ζ enters—in form of the correlation energy $E_\zeta = \hbar^2/m\zeta^2$ —the important energy scale $E_\Delta = V_L^2/E_\zeta$, which determines the minimum energy for weak scattering. The validity of our results is restricted to the regime where the atomic energy is larger than the weak scattering energy E_Δ . In this regime the atoms are only weakly scattered by the speckle fluctuations.

Using a linear response theory, we calculate the weak localization correction to classical transport. These interference corrections are sensitive to phase-breaking mechanisms such as spontaneous photon emission. These spontaneous dissipative processes can be maintained at harmless rates for realistic values of the experimental parameters. We have shown that in this case the weak localization correction δD can reach a considerable fraction of the Boltzmann diffusion constant D_B within the weak scattering regime for atoms at recoil or sub-recoil temperatures. Even the strong localization threshold is within reach of current experimental techniques; we have calculated the corresponding critical disorder values and localization lengths. In order to measure the diffusion constant and its weak localization corrections in an actual experiment, one could for instance release a confined atomic cloud and monitor its long-time spread inside the speckle field by time-of-flight or in-situ imaging techniques. The crossover to the strongly localized regime would appear as a freezing of the diffusive process as the cloud reaches the localization length, with a final density distribution mapping out the longest-lived localized eigenmodes of each realization that permit the corresponding localisation length to be measured.

The extension to non-monochromatic matter wave distributions (such as the ones used in the recent publications [40, 66]) is straightforward and will be the subject of a subsequent publication.

As the use of sub-recoil temperatures favors localization effects, the most promising candidate for matter wave experiments seems to be a Bose-Einstein condensate. In this respect, another extension of this work would be to consider the dynamics of a Bose-Einstein condensate [40] in the 2D and 3D speckle field and to study the role of interactions (for instance using the approach developed in [67]) and quantum statistics on localization. Another possible extension of this work would be to study the influence of the internal spin structure of the atom.

Finally, this work could be extended to disordered magnetic potentials. One immediate advantage compared to the optical speckle potential would be the Gaussian character of the magnetic potential fluctuations [68]. A first numerical study of the expansion of a Bose-Einstein condensate in a one-dimensional disordered atomic waveguide has revealed characteristic signatures of localization in the non-interacting regime [69]. This could open the door to further experiments studying disorder on atom chips [70, 71].

Acknowledgments

We acknowledge financial support from DFG, BFHZ-CCUFB, the PROCOPE and the Marie Curie program. R. Kuhn is particularly indebted to the DAAD for financial support within

the doctoral fellowship program. R. Kuhn would like to thank G. Montambaux for helpful technical discussions and the Institut Non Linéaire de Nice, Laboratoire Kastler Brossel and the Physics Department of the National University of Singapore for their kind hospitality. The authors would like to thank R. Kaiser, D. Wilkowski, G. Labeyrie, T. Chanelière, T. Wellens, B. Grémaud, R. Sapienza, L. Sanchez-Palencia for their interest, and finally an anonymous referee for helpful remarks.

Appendix A. Self-energy Σ and small perturbation parameter

Let us recall the self-energy series (26),

$$\Sigma = \sum_{n \geq 2} \Sigma_n, \quad (\text{A.1})$$

where Σ_n represents all one-propagator irreducible diagrams of order n in field correlations and in powers of $\eta = V_L/E_\zeta$, the speckle strength in units of correlation energy. The first terms are:

$$\Sigma_2 = \bullet \text{---} \bullet =: \otimes \text{---} \otimes \quad (\text{A.2})$$

$$\Sigma_3 = \bullet \text{---} \bullet \text{---} \bullet \quad (\text{A.3})$$

$$\begin{aligned} \Sigma_4 = & \otimes \text{---} \otimes \text{---} \otimes \text{---} \otimes + \otimes \text{---} \otimes \text{---} \otimes \text{---} \otimes \\ & + \bullet \text{---} \bullet \text{---} \bullet \text{---} \bullet + \bullet \text{---} \bullet \text{---} \bullet \text{---} \bullet + \bullet \text{---} \bullet \text{---} \bullet \text{---} \bullet \end{aligned} \quad (\text{A.4})$$

$$\Sigma_5 = \otimes \text{---} \bullet \text{---} \bullet \text{---} \bullet \text{---} \otimes + \bullet \text{---} \bullet \text{---} \bullet \text{---} \bullet \text{---} \bullet + \dots \quad (\text{A.5})$$

In these diagrams, every straight line represents the free propagator G_0 defined in (16). “Irreducible” means that by cutting any such single propagator line, the diagrams do not split into independent parts. A dotted line like $\bullet \cdots \bullet = \eta \gamma_d$ represents the field correlation function (4). A double dotted line $\bullet \cdots \bullet = \eta^2 \mathcal{P}_d = \eta^2 |\gamma_d|^2$ represents the intensity correlation function (6), that we note $\eta^2 \mathcal{P}_d = \otimes \cdots \otimes$ for simplicity in the following. To evaluate a diagram, one writes down its expression in terms of correlation functions and propagators and integrates over all free internal variables. This integration is most conveniently done in momentum space since the free propagator $G_0(\kappa, \varepsilon)$ is then diagonal.

As an example, let us calculate the first diagram $\Sigma_2 = \otimes \text{---} \otimes$ explicitly. The potential fluctuation operator $\otimes = \eta \delta V$ is diagonal in real space and therefore translation invariant in momentum space: $\langle \kappa' | \delta V | \kappa \rangle = \delta V(\kappa - \kappa')$. The Fourier transform of the potential fluctuations is defined by

$$\delta V(\kappa) = \int d^d \rho \delta V(\rho) e^{-i\kappa \cdot \rho}, \quad \delta V(\rho) = \int \frac{d^d \kappa}{(2\pi)^d} \delta V(\kappa) e^{i\kappa \cdot \rho}. \quad (\text{A.6})$$

The 2-point correlation function of the potential fluctuations in momentum space reads

$$\overline{\delta V(\kappa_1) \delta V(\kappa_2)} = (2\pi)^d \delta(\kappa_1 + \kappa_2) \mathcal{P}_d(\kappa_1), \quad (\text{A.7})$$

where $\mathcal{P}_d(\kappa)$ is the Fourier transform of $\mathcal{P}_d(\rho)$ that was defined in (6). The matrix elements of $\Sigma_2(\varepsilon)$ are given by $\langle \kappa' | \Sigma_2(\varepsilon) | \kappa \rangle = (2\pi)^d \delta(\kappa - \kappa') \Sigma_2(\kappa, \varepsilon)$; as expected, the self-energy operator is diagonal in momentum space and isotropic. Its diagonal entries are

$$\Sigma_2(\kappa, \varepsilon) = \eta^2 \int \frac{d^d \kappa_1}{(2\pi)^d} \mathcal{P}_d(\kappa - \kappa_1) G_0(\kappa_1, \varepsilon), \quad (\text{A.8})$$

which is simply the momentum convolution of the potential correlation function \mathcal{P}_d with the free Green function G_0 .

The appearance of odd terms Σ_{2q+1} in the formal series (A.1) reflects the non-Gaussian character of the potential fluctuations. We now wish to determine the effective small parameter and corresponding range of validity of the self-energy series. To this aim, we discuss separately the high-energy and low-energy cases $\kappa = \sqrt{2\varepsilon} \gg 1$ and $\kappa \ll 1$, respectively.

In the high-energy limit, it is possible to determine the dependence of Σ_n on the ultraviolet momentum $\kappa \gg 1$ by simple power counting. Each irreducible diagram contributing to Σ_n contains $n - 1$ internal propagators $G_0(\varepsilon)$, p field-correlation functions ($0 \leq p \leq n$), and $(n-p)/2$ intensity-correlation functions. Taking into account all momentum conservation laws, this leaves exactly $(n+p)/2$ independent variables κ_i that can be chosen to be the arguments $\gamma_d(\kappa_i)$ or $\mathcal{P}_d(\kappa_i)$ of the correlation functions (14a) and (14b). Because of the strict momentum cutoff, these correlation functions constrain the norms κ_i to remain of order unity or smaller. The only dependence on κ comes from the Green functions $G_0(\kappa_m, \varepsilon)$ that are evaluated at momenta $\kappa_m = \kappa - \sum_i \alpha_i \kappa_i$ with coefficients $\alpha_i \in \{0, \pm 1\}$ that describe the diagram's topology. Linearizing around the on-shell value $\varepsilon = \kappa^2/2$ for $\kappa \gg \kappa_i$, each Green's function contributes a power κ^{-1} such that $\Sigma_n \sim a_n \eta^n \kappa^{1-n} = a_n \kappa (\eta/\kappa)^n$, where a_n is related to the number of n -point irreducible diagrams. We thus can identify the effective expansion parameter $g = \eta/\kappa$ that should be small, which in turn justifies the choice of the weak scattering condition $\Delta = \eta^2/\varepsilon = 2g^2 \ll 1$ in section 3.3 above. Of course, such an analysis of a superficial degree of divergence [72] can only determine how the small parameter depends on energy, but not fix numerical factors of order unity. We can rewrite the ratio of the self-energy (A.1) to the kinetic energy ε as

$$\Sigma/\varepsilon \sim \sum_{n \geq 2} \frac{a_n}{\kappa} g^n, \quad (\kappa \gg 1), \quad (\text{A.9})$$

In this high-energy regime, non-Gaussian terms $n = 2q + 1$ contribute to the series. In other words, fast atoms live in a potential that has definitely non-Gaussian statistics beyond the leading-order Born approximation $n = 2$.

The low-energy limit $\kappa \ll 1$ in 2D allows for a similar analysis. Each of the $(n+p)/2$ correlation functions in Σ_n tends towards its finite limit as $\kappa \rightarrow 0$ and thus becomes effectively δ -correlated in real space. The contributions κ^{n+p} from the $(n+p)/2$ integration measures and κ^{2-2n} from the $n-1$ Green's functions yield a scaling κ^{2-n+p} for Σ_n . If n is even, Σ_n is therefore dominated by the diagrams with $p = 0$, containing only intensity-correlation functions and diverging like κ^{2-n} . If n is odd, the dominant contribution comes from the diagrams with the smallest number of field correlations, $p = 3$, that appear first in Σ_3 and reappear subsequently in higher non-Gaussian terms Σ_{2q+1} . One can then rewrite the dominant contributions to (A.1) in the form

$$\Sigma/\varepsilon \sim \sum_{q \geq 1} (a_{2q} g^{2q} + a_{2q+1} \kappa^3 g^{2q+1}), \quad (2\text{D and } \kappa \ll 1). \quad (\text{A.10})$$

Remarkably, $g = \eta/\kappa$ is still the expansion parameter, and remains small if $\eta \ll \kappa \ll 1$. Terms which are negligible compared to both their neighbors in the series can be omitted. This applies to all odd terms when $\kappa^3 g^{2q+1} \ll g^{2q+2}$, i.e. $\kappa^3 \ll g$ at fixed g . In this low-energy and weak-scattering regime, the self-energy does no longer depend on the field-correlation functions, and only the Gaussian terms survive:

$$\Sigma/\varepsilon \sim \sum_{q \geq 1} a_{2q} g^{2q}, \quad (2\text{D and } \kappa^3 \ll g). \quad (\text{A.11})$$

The 3D case requires a separate discussion. As far as the pure intensity correlations ($p = 0$) are concerned, actually the same reasoning as for 2D holds because the low- κ -divergence of the intensity correlation $\propto \kappa^{-1}$ is compensated by a supplementary factor from the integration measure. However, the pure field-correlation functions $\gamma_3(\kappa) = \delta(1 - \kappa)$ cannot tend to a constant as $\kappa \rightarrow 0$, but project all integration momenta onto the unit sphere. Consequently, a small- κ -contribution of the integration measure and the correlation functions can only come from the $(n - p)/2$ variables intervening in the intensity-correlation functions: it reads κ^{n-p} . The contribution of a propagator is either κ^{-2} (as in the 2D case) if it does not depend on a field-correlation momentum, or independent of κ in the limit $\kappa \rightarrow 0$ because field correlation momenta of order unity remain present. Thus, the diagrams depending only on the field-correlations ($n = p$) behave like κ^0 . At fixed n and p , the dominant diagrams mixing field- and intensity-correlation functions are those with the largest number of propagator lines independent of the p field-correlation variables. This happens when field correlations can be written as products of the largest number of independent field-correlation sub-diagrams that never cross the intensity-correlation lines. An example for such a diagram is the first contribution to Σ_5 shown in (A.5) that displays a Σ_3 -type field correlation inside a Σ_2 intensity correlation. In all dominant cases, the field sub-diagrams will contain at most 3, 4 or 5 vertices (as those shown in Σ_3 , Σ_4 , and Σ_5), because higher-order field correlations could be factorized into these elementary ones, thus yielding an additional independent propagator. Writing $p = 3n_1 + 4n_2 + 5n_3$, where the n_i are non-negative integers, the largest possible number of sub-diagrams is obtained by maximizing the sum $n_1 + n_2 + n_3$. The number of propagator lines giving a κ^{-2} contribution to the diagram is then $n - p + n_1 + n_2 + n_3 - 1$, and the total contribution of the diagram is $\kappa^{2-n+n_1+2n_2+3n_3}$. It turns out that when n is even, the dominant contribution κ^{2-n} to Σ_n comes from the intensity-correlation diagrams ($p = 0$). When n is odd, the main contribution κ^{3-n} is due to the diagrams with $n_1 = 1$, i. e. $p = 3$. Similarly to the 2D case, the dominant contribution to the self-energy (A.1) is

$$\Sigma/\varepsilon = \sum_{q \geq 1} (a_{2q} g^{2q} + a_{2q+1} \kappa g^{2q+1}). \quad (\text{A.12})$$

As in the 2D case, $g = \eta/\kappa$ is the expansion parameter. Again, terms which are negligible compared to both their neighbors can be omitted. This applies to the odd terms when $\kappa^2 \ll \eta \ll \kappa \ll 1$ at fixed g , i. e. in the quantum regime discussed at the end of section 3.3. In this regime, an effective δ -correlated Gaussian potential is recovered.

Since the number of diagrams a_n grows factorially with n , we face the well-known troublesome fact that even for $g \ll 1$, our global weak scattering condition covering both the high- and low-energy regime, the series (A.1) formally diverges. It can only be understood as an *asymptotic* series that can be accurately approximated by just the first few terms [73]. When the effective coupling constant g is sufficiently small, then a truncation to the first term already gives a good approximation to the self-energy. The weak scattering condition is thus given by $g \ll 1$, or equivalently by $\eta \ll \kappa$, which amounts to $E \gg E_\Delta = V_L^2/E_\zeta$.

Self-energy diagrams like $\otimes \text{---} \otimes$ and $\otimes \text{---} \otimes \text{---} \otimes$ and similarly nested higher-order diagrams with an outer correlation function can be self-consistently summed up to give the diagram $\otimes \text{---} \otimes$, where the thick line represents the average Green function. The same procedure can be applied to all diagrams like $\otimes \text{---} \otimes \text{---} \otimes$ with two outer correlation functions yielding the self-consistent diagram $\otimes \text{---} \otimes \text{---} \otimes$, etc.

Appendix B. Diffusion from quantum kinetic equation

This appendix is devoted to the derivation of the diffusion constant using a quantum linear response theory that we believe to be a slightly improved version of Vollhardt and Wölfle's approach [38].

Appendix B.1. Quantum kinetic equation and continuity equation

We first rewrite the Bethe-Salpeter equation (50) for the intensity propagator $\Phi(\kappa, \kappa', \mathbf{q}, \varepsilon, \omega)$ in a more useful way. For the scalar quantities the product of the average propagators $\overline{G}^\dagger(\varepsilon_-) \otimes \overline{G}(\varepsilon_+)$ can be reformulated in momentum space by using the identity $\overline{G}^* \overline{G} = (\overline{G}^* - \overline{G})/(\overline{G}^{-1} - \overline{G}^{*-1})$ as

$$\overline{G}^*(\kappa'_-, \varepsilon_-) \overline{G}(\kappa'_+, \varepsilon_+) = \frac{-\Delta G(\kappa', \mathbf{q}, \varepsilon, \omega)}{\omega - \mathbf{q} \cdot \kappa' - \Delta \Sigma(\kappa', \mathbf{q}, \varepsilon, \omega)}, \quad (\text{B.1})$$

where $\kappa'_\pm = \kappa' \pm \mathbf{q}/2$ and $\Delta G(\kappa, \mathbf{q}, \varepsilon, \omega) = \overline{G}(\kappa_+, \varepsilon_+) - \overline{G}^*(\kappa_-, \varepsilon_-)$ as well as $\Delta \Sigma(\kappa, \mathbf{q}, \varepsilon, \omega) = \Sigma(\kappa_+, \varepsilon_+) - \Sigma^*(\kappa_-, \varepsilon_-)$. Multiplying the denominator to the other side leads to the quantum kinetic equation [21]

$$[\omega - \mathbf{q} \cdot \kappa'] \Phi(\kappa, \kappa', \mathbf{q}, \varepsilon, \omega) = -(2\pi)^d \delta(\kappa - \kappa') \Delta G(\kappa', \mathbf{q}, \varepsilon, \omega) + \mathcal{C}[\Phi]. \quad (\text{B.2})$$

This is the standard form of a kinetic equation with a Fourier-transformed drift derivative on the left hand side, and on the right hand side first a source term and then all scattering information contained in the linear collision functional

$$\begin{aligned} \mathcal{C}[\Phi] &= \Delta \Sigma(\kappa', \mathbf{q}, \varepsilon, \omega) \Phi(\kappa, \kappa', \mathbf{q}, \varepsilon, \omega) \\ &\quad - \Delta G(\kappa', \mathbf{q}, \varepsilon, \omega) \int \frac{d^d \kappa''}{(2\pi)^d} \Phi(\kappa, \kappa'', \mathbf{q}, \varepsilon, \omega) U(\kappa'', \kappa', \mathbf{q}, \varepsilon, \omega). \end{aligned} \quad (\text{B.3})$$

As shown by Vollhardt and Wölfle [38], the irreducible vertex U and the self-energy Σ are intimately linked through the Ward identity [21, 38]

$$\Delta \Sigma(\kappa', \mathbf{q}, \varepsilon, \omega) = \int \frac{d^d \kappa''}{(2\pi)^d} \Delta G(\kappa'', \mathbf{q}, \varepsilon, \omega) U(\kappa'', \kappa', \mathbf{q}, \varepsilon, \omega). \quad (\text{B.4})$$

Notably, the proof works also for correlated potentials and thus applies without restriction to our case (in contrast to scattering by resonant potentials where corrections to the Ward identity renormalize the transport speed of the propagating wave [25]). This Ward identity plays the role of an optical theorem: everything that disappears from the forward propagating mode is scattered into other modes. With its help, the scattering functional can be rewritten as

$$\begin{aligned} \mathcal{C}[\Phi] &= \int \frac{d^d \kappa''}{(2\pi)^d} [\Delta G(\kappa'', \mathbf{q}, \varepsilon, \omega) \Phi(\kappa, \kappa', \mathbf{q}, \varepsilon, \omega) \\ &\quad - \Delta G(\kappa', \mathbf{q}, \varepsilon, \omega) \Phi(\kappa, \kappa'', \mathbf{q}, \varepsilon, \omega)] U(\kappa'', \kappa', \mathbf{q}, \varepsilon, \omega). \end{aligned} \quad (\text{B.5})$$

By parity, it vanishes identically under integration over κ' , $\int d^d \kappa' \mathcal{C}[\Phi] = 0$. Moreover, one can verify that $\int d\varepsilon \Delta G(\kappa, \mathbf{q}, \varepsilon, \omega) = 2\pi i$ by going back to the definition of the time-evolution propagator and observing that $U(t=0) = \mathbb{1}$ while defining $\Theta(0) = \frac{1}{2}$. By integrating the quantum kinetic equation over κ' and ε , we thus recover the continuity equation (49) exactly to all orders in \mathbf{q} and ω . This is slightly different from Vollhardt and Wölfle's approach, followed by the entire quantum transport literature, which uses different kernels defined by sums over κ' and κ (instead of κ' and ε) that only obey an approximate continuity equation.

Appendix B.2. Linear response

Starting with the continuity equation, we now need a second equation that expresses the current $\Phi_1(\kappa, \mathbf{q}, \omega)$ as function of a small gradient in density, thus defining a linear-response coefficient. Multiplying the QKE (B.2) by $\mathbf{q} \cdot \kappa'$ and integrating over ε and κ' gives an equation for the current kernel Φ_1 :

$$\begin{aligned} \omega \mathbf{q} \cdot \Phi_1(\kappa, \mathbf{q}, \omega) - \int \frac{d\varepsilon}{2\pi} \int \frac{d^d \kappa'}{(2\pi)^d} (\mathbf{q} \cdot \kappa')^2 \Phi(\kappa, \kappa', \mathbf{q}, \varepsilon, \omega) \\ = -i \mathbf{q} \cdot \kappa + \int \frac{d\varepsilon}{2\pi} \int \frac{d^d \kappa'}{(2\pi)^d} (\mathbf{q} \cdot \kappa') \mathcal{C}[\Phi]. \end{aligned} \quad (\text{B.6})$$

This is not a closed equation for Φ_0 and Φ_1 because it involves higher-order moments of the full distribution Φ . If one continues to write equations for the new unknowns, one generates a hierarchy that must be truncated judiciously in order to extract the density kernel Φ_0 .

In the long time and long-distance limit $q, \omega \rightarrow 0$, we can make two assumptions that facilitate the derivation of the transport time in the linear response regime. Firstly, we perform the usual expansion

$$\tilde{\Phi}(\kappa, \kappa', \mathbf{q}, \varepsilon, \omega) = \frac{A(\kappa', \varepsilon)}{2\pi \mathcal{N}(\varepsilon)} \int \frac{d^d \kappa''}{(2\pi)^d} \left[1 + \frac{d}{2\varepsilon} (\kappa' \cdot \hat{\mathbf{q}})(\hat{\mathbf{q}} \cdot \kappa'') \right] \Phi(\kappa, \kappa'', \mathbf{q}, \varepsilon, \omega) \quad (\text{B.7})$$

into the lowest-order terms in powers of the angular dependence on $\hat{\mathbf{q}} \cdot \kappa'$, isotropic and vectorial. The factorized spectral function $A(\kappa', \varepsilon)$ encapsulates the dependence on the modulus of κ' which is constrained to the disorder-broadened energy shell; indeed, the Bethe-Salpeter equation (50) shows that the intensity relaxation kernel Φ is proportional to $\Delta G(\kappa', \mathbf{q}, \varepsilon, \omega)$ which is itself very well approximated by the strongly peaked spectral function $A(\kappa, \varepsilon)$ since $\Delta G(\kappa, \varepsilon) = 2i \text{Im} \bar{G}(\kappa, \varepsilon) = -iA(\kappa, \varepsilon)$. Secondly, by symmetry in κ and κ' , the intensity relaxation kernel Φ is also proportional to $A(\kappa, \varepsilon)$. As a sharply peaked function of ε , the kernel can therefore be well approximated by $\Phi(\kappa, \kappa'', \mathbf{q}, \varepsilon, \omega) \approx A(\kappa, \varepsilon) \int \frac{d\varepsilon'}{2\pi} \Phi(\kappa, \kappa'', \mathbf{q}, \varepsilon', \omega)$. Using this in (B.7) leads to the ansatz

$$\tilde{\Phi}(\kappa, \kappa', \mathbf{q}, \varepsilon, \omega) = \frac{A(\kappa, \varepsilon)A(\kappa', \varepsilon)}{2\pi \mathcal{N}(\varepsilon)} \left[\Phi_0(\kappa, \mathbf{q}, \omega) + \frac{d}{2\varepsilon} (\kappa' \cdot \hat{\mathbf{q}}) \hat{\mathbf{q}} \cdot \Phi_1(\kappa, \mathbf{q}, \omega) \right]. \quad (\text{B.8})$$

This expression in terms of the relevant kernels Φ_0 and Φ_1 is custom-tailored such that the consistency relations $\tilde{\Phi}_0 = \Phi_0$ and $\tilde{\Phi}_1 = \Phi_1$ hold. We can therefore insert $\Phi \approx \tilde{\Phi}$ into (B.6) and calculate the two remaining terms. On the left-hand side, only the Φ_0 -term gives a contribution since the Φ_1 -term vanishes by parity. On the right-hand side, the collision integral of the isotropic Φ_0 -term vanishes by parity if $\Delta\Sigma$, ΔG , and U are evaluated at $\mathbf{q} = 0$ and $\omega = 0$. This is allowed to leading order in q, ω because the collision integral is already of order $1/\tau_s$. The remaining integral over the Φ_1 -term defines the inverse transport time (52). Rearranging the equation, we can solve for $\mathbf{q} \cdot \Phi_1$ and obtain (51).

Together with the continuity equation (49) this provides a closed set of equations for Φ_0 and Φ_1 with the following solutions for $\omega\tau(\kappa) \ll 1$:

$$\Phi_0(\kappa, \mathbf{q}, \omega) = \frac{1 - i\tau(\kappa)\mathbf{q} \cdot \kappa}{-i\omega + \mathcal{D}(\kappa)q^2}, \quad i\mathbf{q} \cdot \Phi_1(\kappa, \mathbf{q}, \omega) = \frac{\mathcal{D}(\kappa)q^2}{-i\omega + \mathcal{D}(\kappa)q^2} \quad (\text{B.9})$$

with the reduced diffusion constant $\mathcal{D}(\kappa) = \kappa^2 \tau(\kappa)/d$. Inserting these solutions into the expansion (B.8) yields the corresponding diffusive intensity propagation kernel

$$\Phi(\kappa, \kappa', \mathbf{q}, \varepsilon, \omega) = \frac{A(\kappa, \varepsilon)A(\kappa', \varepsilon)}{2\pi \mathcal{N}(\varepsilon)} \frac{1 - i\tau(\kappa)\mathbf{q} \cdot (\kappa + \kappa')}{-i\omega + \mathcal{D}(\kappa)q^2}. \quad (\text{B.10})$$

Appendix C. Intensity diagrams and Boltzmann transport theory

The Bethe-Salpeter equation (50) can be formally recast into the form

$$\Phi = [\overline{G}^\dagger \otimes \overline{G}] + [\overline{G}^\dagger \otimes \overline{G}] R [\overline{G}^\dagger \otimes \overline{G}], \quad (\text{C.1})$$

where the reducible vertex is $R = U + U [\overline{G}^\dagger \otimes \overline{G}] R$. The first terms of the power series $U = \sum_{n \geq 2} U_n$ for the irreducible intensity vertex are the following diagrams:

$$U_2 = \begin{array}{c} \otimes \\ \vdots \\ \otimes \end{array} \quad (\text{C.2})$$

$$U_3 = \begin{array}{c} \bullet \\ \diagup \quad \diagdown \\ \bullet \quad \bullet \end{array} + \begin{array}{c} \bullet \\ \diagup \quad \diagdown \\ \bullet \quad \bullet \end{array} \quad (\text{C.3})$$

$$U_4 = \begin{array}{c} \otimes \quad \otimes \\ \diagup \quad \diagdown \\ \otimes \quad \otimes \end{array} + \begin{array}{c} \otimes \quad \otimes \\ \diagup \quad \diagdown \\ \otimes \quad \otimes \end{array} + \begin{array}{c} \otimes \\ \vdots \\ \otimes \end{array} + \begin{array}{c} \bullet \\ \diagup \quad \diagdown \\ \bullet \quad \bullet \end{array} + \begin{array}{c} \bullet \\ \diagup \quad \diagdown \\ \bullet \quad \bullet \end{array} + \dots \quad (\text{C.4})$$

As before, “irreducible” means that these diagrams do not fall apart into independent sub-diagrams by cutting one of the thick lines that represent the average propagators \overline{G} . The upper lines belong to retarded amplitudes \overline{G} while the lower entries belong to advanced amplitudes \overline{G}^\dagger . Dotted lines connecting two \otimes (resp. \bullet) represent an intensity (resp. field) correlation function. In addition to the familiar potential correlations as in U_2 and U_4 , we find field-correlation diagrams as in U_3 and all higher orders, since the potential fluctuations do not obey Gaussian statistics.

Through the Ward identity (B.4), every self-consistent diagram in the expansion of the self-energy corresponds to a set of diagrams in the expansion of U . For example, the diagram (C.2) is linked to the self-consistent diagram $\otimes \text{---} \otimes$, exactly as in the electronic case. This means in particular that the Boltzmann approximation $U \approx U_B = U_2$ and the weak scattering approximation $\Sigma \approx \Sigma_2$ are consistent, and the Ward identity (B.4) appears as the expression (34) of the scattering mean free path in terms of the Boltzmann vertex (58). The next two diagrams (C.3) are linked to the field correlations $\bullet \text{---} \bullet$ defining Σ_3 , and the following (C.4) are linked to $\otimes \text{---} \otimes$, etc.

In the Boltzmann approximation $U = U_2$, the reducible vertex at the core of the intensity propagator (C.1) becomes $R_B = U_2 + U_2 [\overline{G}^\dagger \otimes \overline{G}] U_2 + \dots = U_2 + L$. Here L denotes the so-called *diffuson*, the letter L referring to the ladder topology of diagrams:

$$L = \begin{array}{c} \otimes \quad \otimes \\ \diagup \quad \diagdown \\ \otimes \quad \otimes \end{array} + \begin{array}{c} \otimes \quad \otimes \\ \diagup \quad \diagdown \\ \otimes \quad \otimes \end{array} + \dots =: \begin{array}{c} \otimes \quad \otimes \\ \diagup \quad \diagdown \\ \otimes \quad \otimes \end{array} \quad (\text{C.5})$$

We will need an analytical expression for the diffuson in the diffusive regime. To this end, we consider the geometric series for Φ_B in the Boltzmann approximation:

$$\Phi_B = \begin{array}{c} \text{---} \\ \text{---} \end{array} + \begin{array}{c} \otimes \\ \diagup \quad \diagdown \\ \otimes \end{array} + \begin{array}{c} \otimes \quad \otimes \\ \diagup \quad \diagdown \\ \otimes \quad \otimes \end{array} \quad (\text{C.6})$$

The first term on the right-hand side describes ballistic propagation, whereas the second term describes single scattering in the effective medium. These two terms can be neglected compared to the remaining diffuson contribution to the series which is given by (B.10) with $\mathcal{D} = \mathcal{D}_B$. Making use of the identity (B.1) in the long time and large distance limit, i. e. for $\omega = 0$ and $\mathbf{q} = 0$, the spectral functions in (B.10) can be expressed as

$A(\kappa, \varepsilon) = \overline{G^*}(\kappa, \varepsilon) \overline{G}(\kappa, \varepsilon) / \tau_s$. Both spectral functions $A(\kappa, \varepsilon)$ and $A(\kappa', \varepsilon)$ each contribute a factor $1/\tau_s$. The products of the retarded and the advanced Green functions as functions of κ and κ' can be identified with the entering and exiting propagators to the diffuson (C.5) in (C.6). The diffuson is therefore given by

$$L(\kappa, \kappa', \mathbf{q}, \varepsilon, \omega) = \frac{1}{2\pi\mathcal{N}(\varepsilon)\tau_s^2} \frac{1 - i\tau(\kappa)\mathbf{q} \cdot (\kappa + \kappa')}{-i\omega + \mathcal{D}_B(\kappa)q^2}. \quad (\text{C.7})$$

Only the prefactor differs from the diffusive intensity propagation kernel (B.10). In particular, the diffuson displays the same diffusive pole as the diffusive intensity propagation kernel.

Appendix D. Weak localization correction for anisotropic scattering

The weak localization correction to the transport time (52) is contained in the intensity scattering vertex $U = U_B + C$, where C incorporates the full *cooperon* contribution

$$C = C_A + C_B + C_C \quad (\text{D.1})$$

The momentum diagrams corresponding to these three contributions are

$$C = \text{Diagram 1} + \text{Diagram 2} + \text{Diagram 3} =: \text{Diagram 4} \quad (\text{D.2})$$

Special attention has to be paid to the cooperon contribution in the case of anisotropic scattering. The simple substitution $U = U_B + C_A$ which is sometimes used in the literature (cf. [53]) is not sufficient in this case. For electron transport in highly anisotropic systems Wölfle and Bhatt [74] have performed the calculation of the cooperon contribution for the conductivity tensor. In this calculation the two additional conductivity diagrams C_B and C_C corresponding to dressed Hikami boxes [20] are taken into account. This calculation for the anisotropic conductivity tensor is similar to the calculation of the weak localization correction to the diffusion constant that we wish to perform. We therefore need to include the same additional Hikami diagrams C_B and C_C adapted to our case.

The total transport time including the weak localization correction takes the form:

$$\begin{aligned} \frac{\tau_B}{\tau^*(\kappa)} &= \frac{\tau_B}{\tau_A^*(\kappa)} + \frac{\tau_B}{\tau_s^2} \int \frac{d\varepsilon}{2\pi} \frac{A(\kappa, \varepsilon)}{2\pi\mathcal{N}(\varepsilon)} \int \frac{d^d\kappa'}{(2\pi)^d} \frac{d^d\kappa''}{(2\pi)^d} \\ &\times \left[[\overline{G}(\kappa')]^2 \overline{G^*}(\kappa') [\overline{G}(\kappa'')]^2 \overline{G^*}(\kappa'') + \overline{G}(\kappa') [\overline{G^*}(\kappa')]^2 \overline{G}(\kappa'') [\overline{G^*}(\kappa'')]^2 \right] \\ &\times (1 + \hat{\kappa}' \cdot \hat{\kappa}'') \mathcal{P}_d(\kappa' - \kappa'') \int \frac{d^dQ}{(2\pi)^d} L_0(\kappa, Q, \omega) \end{aligned} \quad (\text{D.3})$$

where the energy dependence of ε of the Green functions has been left out for better visibility and where

$$L_0(\kappa, Q, \omega) = \frac{1}{2\pi\mathcal{N}(\varepsilon)\tau_s^2} \frac{1}{-i\omega + \mathcal{D}_B(\kappa)Q^2}. \quad (\text{D.4})$$

In order to evaluate the integral over κ' and κ'' in (D.3) one makes use of the peaked structure of the Green functions as a function of κ' and κ'' around the point $\kappa_\varepsilon = \sqrt{2\varepsilon}$ for weak

disorder. To leading order in the small disorder parameter $1/\varepsilon\tau_s \ll 1$ the integral over κ' and κ'' then yields:

$$\frac{\tau_B}{\tau^*(\kappa)} = 1 + \frac{\tau_B}{\tau_s^2} \int \frac{d\varepsilon}{2\pi} \frac{A(\kappa, \varepsilon)}{2\pi\mathcal{N}(\varepsilon)} \int \frac{d^d Q}{(2\pi)^d} L_0(\kappa, Q, \omega) \times \left[2[f^{2,2}] + \int \frac{d\Omega'_d}{\Omega'_d} (1 + \hat{\kappa}' \cdot \hat{\kappa}'') \mathcal{P}_d(\kappa_\varepsilon, \theta) \left[[f^{2,1}]^2 + [f^{1,2}]^2 \right] \right]. \quad (\text{D.5})$$

The function $f^{n,m}(\tau_s)$ is defined by [20]:

$$f^{n,m}(\tau_s) = 2\pi\mathcal{N}_0 i^{n-m} \frac{(n+m-2)!}{(m-1)!(n-1)!} (\tau_s)^{n+m-1}. \quad (\text{D.6})$$

Reinserting the functions $f^{n,m}(\tau_s)$ into (D.5), the term in brackets yields the factor $4\pi\mathcal{N}_0\tau_s^3(1 - \langle \cos \theta \rangle)$. Evaluating the integral over ε to leading order in $1/\varepsilon\tau_s$, we obtain the final result

$$\frac{\tau_B}{\tau^*(\kappa)} = 1 + \frac{1}{\pi\mathcal{N}_0(\varepsilon_\kappa)} \int \frac{d^d Q}{(2\pi)^d} \frac{1}{-i\omega + \mathcal{D}_B(\kappa)Q^2} \quad (\text{D.7})$$

that leads to the corrected inverse diffusion constant (66).

References

- [1] M. Lewenstein, A. Sanpera, V. Ahufinger, B. Damski, A. Sen De, and U. Sen, *Adv. Phys.* 56: 243, 2007
- [2] F. Dalfovo, S. Giorgini, L.P. Pitaevskii and S. Stringari, *Rev. Mod. Phys.*, 71:463, 1999.
- [3] R. Kaiser, C. Westbrook, and F. David. *Les Houches, Session LXXII, Coherent atomic matter waves*. Springer-Verlag, Berlin, 2001.
- [4] R. A. Duine and H. T. C. Stoof. *Phys. Rep.*, 396:115, 2004.
- [5] S. Sachdev. *Quantum Phase Transitions*. Cambridge University Press, Cambridge, 2001.
- [6] V. Ahufinger, L. Sanchez-Palencia, A. Kantian, A. Sanpera, and M. Lewenstein. *Phys. Rev. A*, 72:063616, 2005.
- [7] M. P. A. Fisher, P. B. Weichman, G. Grinstein, and D. S. Fisher. *Phys. Rev. B*, 40:546, 1989.
- [8] P. Lugan, D. Clément, P. Bouyer, A. Aspect, M. Lewenstein, L. Sanchez-Palencia, *Phys. Rev. Lett.* 98: 170403, 2007
- [9] B. Damski, J. Zakrzewski, L. Santos, P. Zoller, and M. Lewenstein. *Phys. Rev. Lett.*, 91:080403, 2003.
- [10] J. E. Lye, L. Fallani, M. Modugno, D. S. Wiersma, C. Fort, and M. Inguscio. *Phys. Rev. Lett.*, 95:070401, 2005.
- [11] D. Clément, A. F. Varón, J. A. Retter, P. Bouyer, L. Sanchez-Palencia, D. M. Gangardt, G. V. Shlyapnikov, and A. Aspect. *Phys. Rev. Lett.*, 95:170409, 2005.
- [12] C. Fort, L. Fallani, V. Guarrera, J. E. Lye, M. Modugno, D. S. Wiersma, and M. Inguscio. *Phys. Rev. Lett.*, 95:170410, 2005.
- [13] T. Schulte, S. Drenkelforth, J. Kruse, W. Ertmer, J. Arlt, K. Sacha, J. Zakrzewski, and M. Lewenstein. *Phys. Rev. Lett.*, 95:170411, 2005.
- [14] D. Clément, A. F. Varón, M. Hugbart, J. A. Retter, L. Sanchez-Palencia, A. Aspect, and P. Bouyer. *New Journal of Physics*, 8:165, 2006.
- [15] J. W. Goodman. In J. C. Dainty, editor, *Laser speckle and related phenomena*. Springer-Verlag, 1975.
- [16] L. Fallani, J. E. Lye, V. Guarrera, C. Fort, and M. Inguscio, *Phys. Rev. Lett.* 98: 130404, 2007
- [17] L. Guidoni, C. Triché, P. Verkerk, and G. Grynberg, *Phys. Rev. Lett.*, 79:3363, 1997; L. Guidoni, B. Dépret, A. di Stefano, and P. Verkerk. *Phys. Rev. A*, 60(6):R4233, 1999.
- [18] L. Sanchez-Palencia and L. Santos. *Phys. Rev. A*, 72:053607, 2005.
- [19] E. Akkermans, G. Montambaux, J. L. Pichard, and J. Zinn-Justin. *Proceedings of the Les Houches Summer School, Session LXI, Mesoscopic quantum physics*. North Holland, Elsevier Science, Amsterdam, 1995.
- [20] E. Akkermans and G. Montambaux. *Physique mésoscopique des électrons et des photons*. EDP Sciences, CNRS Editions, Paris, 2004.
- [21] J. Rammer. *Quantum Transport Theory*. Perseus Books, Reading, Mass., 1998.
- [22] G. Bergmann. *Phys. Rep.*, 107:1, 1984.
- [23] P. A. Lee and T. V. Ramakrishnan. *Rev. Mod. Phys.*, 57:287, 1985.
- [24] M. C. W. van Rossum and Th. M. Nieuwenhuizen. *Rev. Mod. Phys.*, 71(1):313, 1999.
- [25] A. Lagendijk and B. A. van Tiggelen. *Phys. Rep.*, 270:143, 1996.
- [26] N. Ashcroft and D. Mermin. *Solid State Physics*. Saunders College, Philadelphia, 1976.

- [27] A. Ishimaru. *Wave propagation and scattering in random media*. IEEE Press, New York, 1997.
- [28] S. Chandrasekhar. *Radiative Transfer*. Dover Publications, New York, 1960.
- [29] P. W. Anderson. *Phys. Rev.*, 109:1492, 1958.
- [30] E. Abrahams, P. W. Anderson, D. C. Licciardello, and T. V. Ramakrishnan. *Phys. Rev. Lett.*, 42:673, 1979.
- [31] B. A. van Tiggelen. In J.-P. Fouque, editor, *Diffusive waves in complex media*. Kluwer Academic Publishers, NATO Science Series, Dordrecht, 1999.
- [32] N. F. Mott. *Metal-Insulator Transitions*. Taylor & Francis, London, 1990.
- [33] B. Kramer and A. MacKinnon. *Rep. Prog. Phys.*, 56:1469, 1993.
- [34] J. Kroha, T. Kopp, and P. Wölfe. *Rhys. Rev. B*, 41:888, 1990.
- [35] T. Kopp. *J. Phys. C: Solid State Phys.*, 17:1897, 1984, and *ibid.*, 17:1919, 1984.
- [36] C. Henkel. 2005. *Preprint: physics/0505023*.
- [37] E. Timmermans, P. Tommasini, M. Hussein, and A. Kerman. *Phys. Rep.*, 315:199, 1999.
- [38] D. Vollhardt and P. Wölfe. *Phys. Rev. B*, 22(10):4666, 1980.
- [39] R. C. Kuhn, C. Miniatura, D. Delande, O. Sigwarth, and C. A. Müller. *Phys. Rev. Lett.*, 95:250403, 2005.
- [40] L. Sanchez-Palencia, D. Clément, P. Lugan, P. Bouyer, G.V. Shlyapnikov, A. Aspect, *Phys. Rev. Lett.* 98: 210401, 2007
- [41] P. Horak, J.-Y. Courtois, and Gilbert Grynberg. *Phys. Rev. A*, 58(5):3953, 1998.
- [42] C. Cohen-Tannoudji, J. Dupont-Roc, and G. Grynberg. *Atom-Photon Interactions: Basic Processes and Applications*. Wiley, New York, 1998.
- [43] Y. Bidet, B. Klappauf, J. C. Bernard, D. Delande, G. Labeyrie, C. Miniatura, D. Wilkowski, and R. Kaiser. *Phys. Rev. Lett.*, 88(20):203902, 2002.
- [44] O. Sigwarth, G. Labeyrie, T. Jonckheere, D. Delande, R. Kaiser, and C. Miniatura. *Phys. Rev. Lett.* 93:143906, 2004.
- [45] L. Allen and J. H. Eberly. *Optical resonance and two-level atoms*. Dover Publications, New York, 1987.
- [46] L. Mandel and E. Wolf. *Optical coherence and quantum optics*. Cambridge University Press, Cambridge, 1996.
- [47] M. Born and E. Wolf. *Principles of Optics*. Cambridge University Press, Cambridge, 1998.
- [48] D. Boiron, C. Mennerat-Robilliard, J.-M. Fournier, J.-M. Guidoni, C. Salomon, and G. Grynberg. *Eur. Phys. J. D*, 7:373, 1999.
- [49] D. Clément, A.F. Varón, J.A. Retter, L. Sanchez-Palencia, A. Aspect, P. Bouyer, *New J. Phys.*, 8:165, 2006.
- [50] M. V. Berry. *J. Phys. A: Math. Gen.*, 10(12):2083, 1977.
- [51] A. Apostol and A. Dogariu. *Phys. Rev. Lett.*, 91:093901, 2003.
- [52] H. Perrin, Y. Colombe, B. Mercier, V. Lorent, and C. Henkel. *J. Phys. B: At. Mol. Opt. Phys.*, 39:4649, 2006.
- [53] P. Sheng. *Introduction to wave scattering, localization and mesoscopic phenomena*. Academic Press, 1995.
- [54] B. A. van Tiggelen and H. Stark. *Rev. Mod. Phys.*, 72(4):1017, 2000.
- [55] U. Frisch. In A. T. Bharucha-Reid, editor, *Probabilistic methods in applied mathematics*. Academic Press, New York, 1968.
- [56] G. D. Mahan. *Many Particle Physics*. Springer-Verlag, Berlin, 1990.
- [57] C. S. Adams, M. Sigel, and J. Mlynek. *Phys. Rep.*, 240:145, 1994.
- [58] C. Henkel, J.-Y. Courtois, and A. Aspect. *J. Phys. II France*, 4:1955, 1994.
- [59] A. Galindo and P. Pascual. *Quantum Mechanics I*. Springer-Verlag, Berlin, 1991.
- [60] S. John. *Phys. Today*, 5:32, 1991.
- [61] J. S. Langer and T. Neal. *Phys. Rev. Lett.*, 16:984, 1966.
- [62] G. M. Minkov, A. V. Germanenko, O. E. Rut, A. A. Sherstobitov, and B. N. Zvonkov. 2006. *Preprint: cond-mat/0606566*.
- [63] W. H. McCrea and F. J. W. Whipple. *Proc. Roy. Soc. Edinburgh*, 60:281, 1940.
- [64] C. Domb. *Proc. Cambridge Philos. Soc.*, 50:586, 1954.
- [65] D. Vollhardt and P. Wölfe. In W. Hanke and Y. V. Kopaev, editors, *Electronic phase transitions*. Elsevier Science B. V., Amsterdam, 1992.
- [66] B. Shapiro, *Preprint: cond-mat/0701346*
- [67] L. Sanchez-Palencia, *Phys. Rev. A*, 74:053625, 2006.
- [68] D. W. Wang, M. D. Lukin, and E. Demler. *Phys. Rev. Lett.*, 92:076802, 2004.
- [69] T. Paul, P. Leboeuf, N. Pavloff, K. Richter, and P. Schlagheck. *Phys. Rev. A*, 72:063621, 2005.
- [70] R. Folman, P. Krüger, D. Cassettari, B. Hessmo, T. Maier, and J. Schmiedmayer. *Phys. Rev. Lett.*, 84:4749, 2000.
- [71] J. Estève, C. Aussibal, T. Schumm, C. Figl, D. Mailly, I. Bouchoule, C. I. Westbrook, and A. Aspect. *Phys. Rev. A*, 70:043629, 2004.
- [72] M. Le Bellac. *Quantum and Statistical Field Theory*. Oxford University Press, 1992.
- [73] C. M. Bender and S. A. Orszag. *Advanced Mathematical Methods for Scientists and Engineers*. Springer-Verlag, New York, 1999.
- [74] P. Wölfe and R. N. Bhatt. *Phys. Rev. B*, 30:3542, 1984.